Volume 43
Number 4
April 2026
Pages 579–780

# Natural Product Reports

rsc.li/npr


ISSN 0265-0568

ROYAL SOCIETY OF CHEMISTRY

**REVIEW ARTICLE**

Roderich D. Süssmuth, Mark Brönstrup *et al.*
A novel class of oligoarylamide antibiotics defined by albicidins and cystobactamids

Natural Product Reports

ROYAL SOCIETY OF CHEMISTRY

REVIEW

View Article Online
View Journal | View Issue



Cite this: *Nat. Prod. Rep.*, 2026, **43**, 597

# A novel class of oligoarylamide antibiotics defined by albicidins and cystobactamids

Marcel Kulike-Koczula, †[a] Dominik Heimann,†[b] Tobias Eulberg, [a] Daniel Kohnhäuser,[b] Roderich D. Süssmuth *[a] and Mark Brönstrup *[bcd]

Received 17th July 2025

DOI: 10.1039/d5np00053j

rsc.li/npr

Covering: 2014/2015 up to 2025.

The global rise of antimicrobial resistance imposes a strong demand to develop new antibacterial drugs, and microbes have been a prime source for their discovery. Albicidins and cystobactamids, isolated from xanthomonadaceae and myxococcaceae, respectively, span a novel class of oligoarylamide antibiotics with a unique chemical scaffold featured by *para*-aminobenzoic acid building blocks. Both compounds exhibit broad spectrum and potent activity against Gram-positive and Gram-negative pathogens through inhibiting DNA gyrase and topoisomerase IV. This article summarizes the insights gained on this class since its initial disclosure in 2014/2015 up to 2025. It discusses natural derivatives, their biosynthesis and chemical synthesis, the unique binding mode to DNA gyrase, and systematic medicinal chemistry programs with >700 analogs that led to resistance-breaking antibiotics with *in vivo* efficacy. The review illustrates the importance of natural product research to address the global need for new antibiotics.



[a]*Department of Chemistry, Technische Universität Berlin, Berlin, 10623, Germany. E-mail: roderich.suessmuth@tu-berlin.de*

[b]*Department of Chemical Biology, Helmholtz Centre for Infection Research, Braunschweig, 38124, Germany. E-mail: mark.broenstrup@helmholtz-hzi.de*

[c]*Institute of Organic Chemistry, Leibniz Universität Hannover, Hannover, 30167, Germany*

[d]*German Center for Infection Research, Site Hannover-Braunschweig, Germany*

† These authors contributed equally.

## 1 Introduction

Antimicrobial resistance (AMR) has been recognized as a major threat for human health that is projected to account for more than 39 million deaths from today until 2050.[1] At the same time, the pace of discovery of new antibiotics has declined, in particular due to a lack of economic incentives for pharmaceutical companies. This results in a current antibiotic pipeline that is too small overall and dominated by improved derivatives from existing drug classes. Although there are notable examples of chemical innovation at both clinical and preclinical stages, there remains a high demand for antibiotics with novel chemical scaffolds and distinct molecular mechanisms of action.[2–4] The underlying assumption is that such compounds are less

sensitive towards existing resistance mechanisms, thereby increasing the arsenal of last resort, resistance-breaking drugs.

Natural products have been – and continue to be – a prime source of antibiotics.[5,6] This is perfectly illustrated by the natural oligoarylamides presented herein. They comprise two different subclasses, the albicidins and the cystobactamids, whose structures were elucidated independently and reported in 2014. Since then, numerous studies on their biosynthesis, chemical synthesis, structural optimization, mechanism of antibiotic action and resistance mechanisms have greatly enhanced our understanding of oligoarylamides and led to the identification of advanced, resistance-breaking antibiotic leads with *in vivo* efficacy. The current review summarizes these efforts by highlighting individual findings for each subclass as well as common features shared by both series.

### 1.1 Discovery of albicidin

The discovery of albicidin dates back to 1985, when it was initially identified as a virulence factor of its producer, the plant pathogen *Xanthomonas albilineans*.[7,8] This group of Gram-negative bacteria causes leaf scald disease in sugarcane, which is discernible by bleached lines along the xylem of leaves ("albilineans" = white-lined) of the plant.[9] Occasionally, toxins of phytopathogens show antibacterial activity,[10] due to the evolutionary relationship of chloroplasts and procaryotes.[11] Subsequent research revealed that isolates capable of causing chlorosis in sugarcane produced an unknown antimicrobial compound with a molecular mass of 842 Da, which was named albicidin.[8] This bactericidal component blocked the replication of chloroplasts and *Escherichia coli* by inhibition of DNA gyrase.[12] The potent antibacterial activity against Gram-negative and Gram-positive bacteria,[8,13] such as *E. coli*, *Acinetobacter baumannii*, *Pseudomonas aeruginosa*, *Enterobacter aerogenes*, *Haemophilus influenzae*, *Staphylococcus aureus* and *Enterococcus faecium*, triggered a high interest to elucidate the structure of this potentially new antibiotic. However, the extremely low fermentation yield of albicidin's natural producer (*ca.* 1 mg from several hundred liters of fermentation broth), heavily impeded isolation attempts. Ultimately, the structure was

**Marcel Kulike-Koczula**

*Marcel Kulike-Koczula was born and raised in Berlin. He studied chemistry at the Technische Universität Berlin, where he completed his master's degree. In 2020, he joined the group of Professor Roderich Süssmuth as a doctoral student. His dissertation focuses on the synthesis and characterization of natural product analogs in the context of medicinal chemistry. His research interests include organic synthesis, antibacterials, medicinal chemistry, and molecular biology.*

**Dominik Heimann**

*Dominik Heimann studied Pharmacy at the University of Münster, where he also obtained his doctorate in Natural Sciences with a focus on Medicinal Chemistry. From 2018 to 2020, he pursued postdoctoral research at the Sanford Burnham Prebys Medical Discovery Institute in San Diego, California. Since 2020, he has been a researcher at the Helmholtz Centre for Infection Research in Brunswick. His scientific interests lie in the design, synthesis, and development of novel antibacterials and antivirals.*

**Tobias Eulberg**

*Tobias Eulberg earned his BSc in Biochemistry from the University of Greifswald in 2020. He went on to complete his MSc in Biological Chemistry at the Technical University of Berlin in 2023. He is currently pursuing a PhD in the laboratory of Prof. Roderich Süssmuth at TU Berlin, where his research focuses on antibiotic resistance against albicidin. By investigating the molecular mechanisms underlying resistance, he aims to contribute to the development of new strategies to overcome antimicrobial challenges.*

**Daniel Kohnhäuser**

*Daniel Kohnhäuser studied Pharmacy at the Goethe University Frankfurt. He obtained his doctorate in chemistry at the Leibniz University Hannover and has been a researcher at the Helmholtz Center for Infection Research since 2018. The focus of his research lies on the design, synthesis and optimization of natural derived antibacterials.*

 

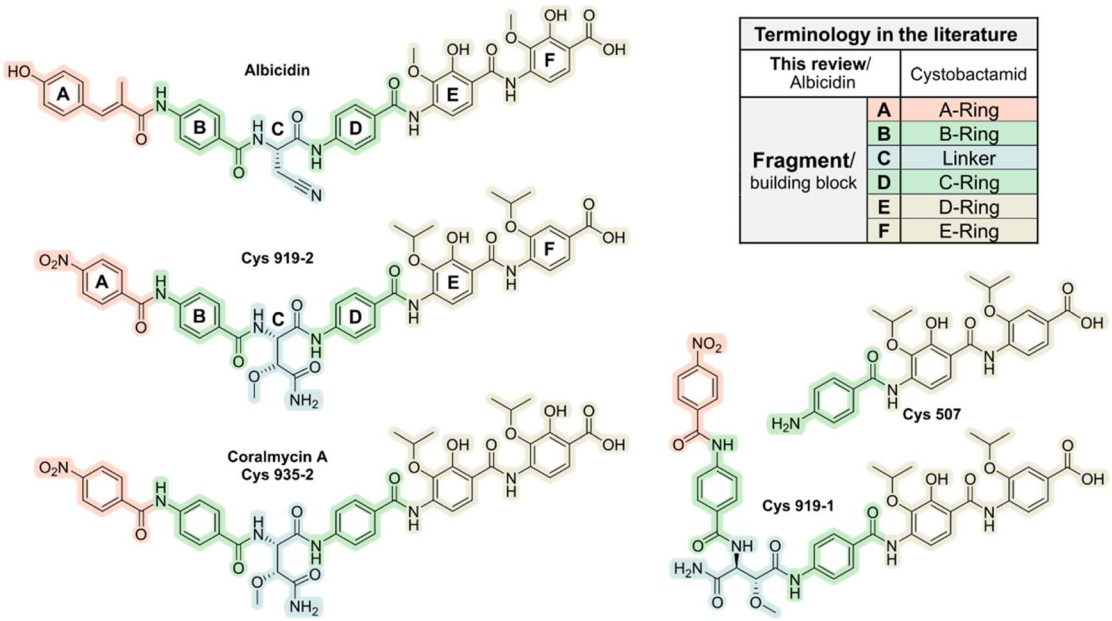


Fig. 1 Chemical structures of albicidin, cystobactamid 919-1, 919-2 and 507 as well as coralmycin A/Cys 935-2. Typically, oligoarylamide antibiotics consist of six fragments that are assigned to the letters A–F. This nomenclature is used throughout this review. In the cystobactamid literature, the fragments are termed A-, B-, C-, D- and E-rings, while the α-amino acid is denoted as "linker". Indicated in red are the N-terminal acyl-functions, in green unsubstituted *p*ABA units, in gold substituted *p*ABA units and in blue the central α-amino acid.

elucidated by a combination of high-resolution tandem mass spectrometry (HR-MS/MS) and 2D nuclear magnetic resonance (NMR) analysis relying on $^{15}$N- and $^{13}$C-labelled albicidin from isotope feeding experiments.[14] The data revealed that albicidin was primarily composed of substituted and unsubstituted *para*-aminobenzoic acids (*p*ABA) (Fig. 1). The central β-cyano-L-alanine (L-Cya) is flanked by two *p*ABA moieties which are connected to a methyl coumaric acid (MCA) at the N-terminus and two 4-amino-2-hydroxy-3-methoxybenzoic acids (*p*MBA) at the C-terminus. These six building blocks connected by amide bonds are assigned to the letters A–F. This nomenclature will be used throughout the review for all oligoarylamides, despite other schemes used in the primary literature (Fig. 1). Subsequent analyses of naturally occurring albicidin-producing strains, using a combination of LC-MS/MS and a spectral networking platform, revealed additional albicidin derivatives (see section Biosynthesis and natural derivatives).

**Roderich D. Süssmuth**

*Roderich D. Süssmuth studied chemistry at the University of Tübingen and received his PhD with Professor Günther Jung. After a post-doctoral stay with Carlos Barbas and Richard Lerner at The Scripps Research Institute (San Diego, CA, USA), he habilitated in Organic Chemistry and Biochemistry at Tübingen University. Since 2004, he has been the Rudolf-Wiechert-Professor of Biological Chemistry at the Technical University of Berlin. His research interests are the discovery and biosynthetic investigations of secondary metabolites, biological and chemical peptide synthesis, and medicinal chemistry.*

**Mark Brönstrup**

*Mark Brönstrup studied Chemistry at the Philipps-Universität Marburg and at Imperial College in London and received his doctorate from the Technical University Berlin in Organic Chemistry. He worked at Sanofi and its predecessor companies from 2000 to 2013, complemented by a research sabbatical in 2003 at Harvard Medical School. Since December 2013, he heads the department Chemical Biology at the Helmholtz Centre for Infection Research; additionally, he holds a Professorship (W3) at the Leibniz Universität Hannover and is a Professor at the German Center for Infection Research (DZIF). His research is focused on the discovery and the characterization of novel antiinfective drugs. He is a member of the Advisory Board of NPR.*

### 1.2 Discovery of cystobactamids

The discovery of the cystobactamids by Müller and coworkers began with the search for antibacterial effects of crude myxobacterial extracts, obtained after small-scale cultivation. The crude extract of the myxobacterium *Cystobacter* sp. Cbv34 was found to inhibit the growth of several Gram-positive and Gram-negative bacteria. After scaling up the fermentation, the three cystobactamids **Cys 919-1**, **Cys 919-2** and **Cys 507**, named after their producer strain and molecular masses, were isolated and analyzed *via* spectroscopic and spectrometric methods to elucidate their chemical structure (Fig. 1).[15] Cystobactamid 919-2 was found to be the most active compound against a panel of five species including *A. baumannii*, *E. coli*, and *S. aureus*. Similar to albicidin, **Cys 919-1** and **Cys 919-2** contain five aromatic systems, connected by a central amino acid serving as a hinge.[15] The latter links the *para*-nitrobenzoic acid (*p*NBA) of fragment A and *p*ABA of fragment B to the *p*ABAs of the fragments D–F either by a (2*S*,3*R*)-β-methoxy-L-asparagine (β-MeO-L-Asn) moiety as in **Cys 919-2**, or by iso-(2*S*,3*R*)-α-methoxy-L-asparagine (α-MeO-L-isoAsn) as in **Cys 919-1**.[16] **Cys 507** is an N-terminally truncated product consisting of rings D–F.[17,18] Independently, Kim *et al.* investigated the metabolites of the myxobacterial strain *Corallococcus coralloides* M23. In addition to **Cys 919-2**, they reported two novel analogues named coralmycin A and B with high structural resemblance to the cystobactamids (Fig. 1).[19]

Major structural differences between cystobactamids and albicidins concern (i) the N-terminus, with a *p*NBA in cystobactamids instead of N-terminal MCA, (ii) the aliphatic amino acid (fragment C), which is L-Cya in albicidins and β-MeO-L-Asn in active cystobactamids, and (iii) the presence of isopropyl ethers in fragments E and F of cystobactamids instead of methyl ethers found in albicidins.

In summary, the discovery of albicidin and cystobactamids from taxonomically unrelated producers belonging to different phyla, *i.e.* myxococcota and pseudomonadota, by three independent groups within a short time frame is remarkable. This coincidence helped to rapidly expand the understanding of the chemistry and biology of oligoarylamide antibiotics in less than a decade.

## 2 Biosynthesis and natural derivatives

Cystobactamids are the products of nonribosomal peptide synthetases (NRPSs), whereas albicidins are synthesized by a hybrid polyketide synthase/nonribosomal peptide synthetase (PKS/NRPS) complex. NRPSs are large, modular enzyme complexes responsible for the ribosome-independent biosynthesis of diverse bioactive peptides containing non-canonical amino acids. The modular nature of NRPSs enables the

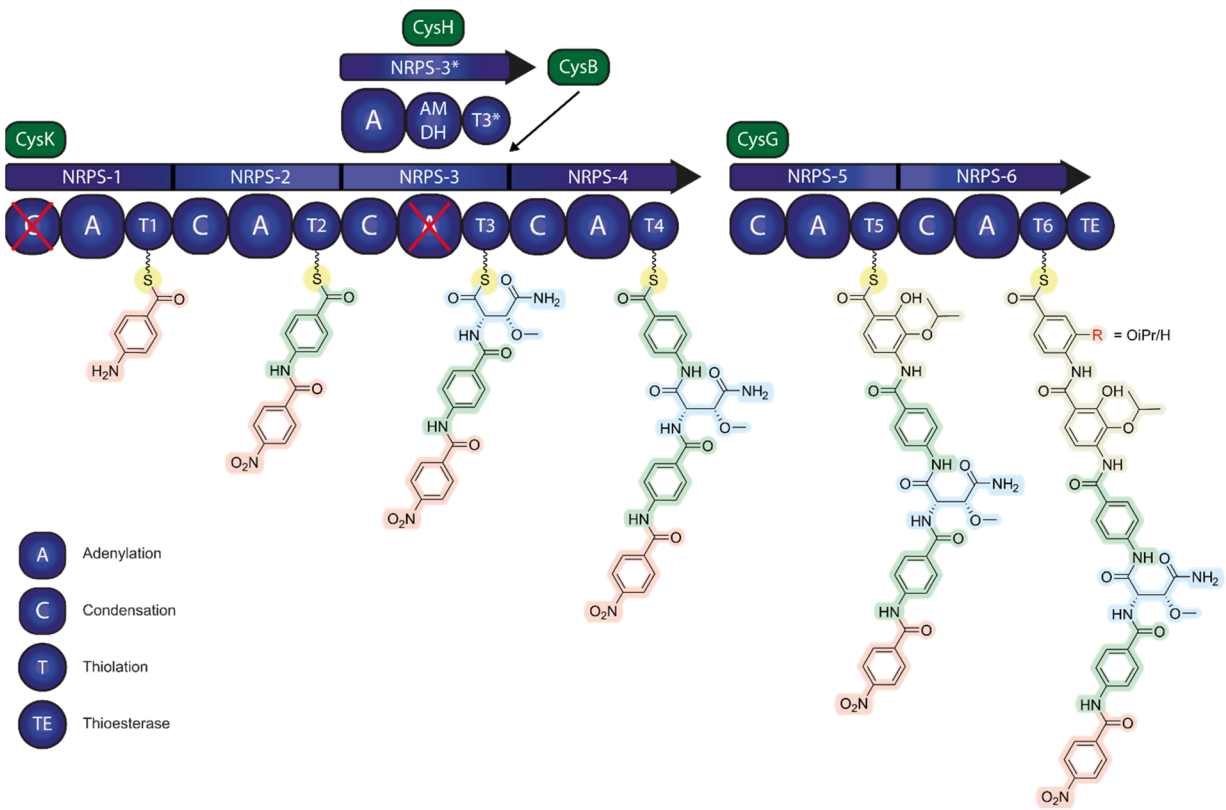


Fig. 2 Model of cystobactamid 919-2 (R = OiPr) and cystobactamid 861-2 (R = H) biosynthesis. The assembly line is encoded by *cysK* and *cysG* with the modules NRPS-1-NRPS-6 (blue arrows). The *p*ABAs of fragments A and B are installed by NRPS-1 and NRPS-2, respectively. β-MeO-L-Asn (biosynthesis shown in Fig. 3) is transferred from T3* of CysH to T3 of CysK by CysB. Another *p*ABA is incorporated by NRPS-4. CysG incorporates the fragments E and F, whereby NRPS-5 recognizes *para*-amino-2-isopropoxy-3-dihydroxybenzoic acid (*p*AIHBA) and NRPS-6 *para*-amino-2-isopropoxybenzoic acid (*p*AIBA) or *p*ABA. The biosynthesis of these building blocks is shown in Fig. 5.

 

biosynthesis of structurally complex peptides with significant pharmaceutical relevance.[20,21]

The biosynthetic gene cluster encoding cystobactamids spans approximately 52 kb and encodes 25 genes. It contains an aminodeoxychorismate (ADC) synthase and the ADC lyase homologues, both required for the synthesis of *p*ABA building blocks. The central β-MeO-L-Asn of **Cys 919-2** is synthesized from L-Asn by the T3*-domain of CysH, followed by CysJ-mediated hydroxylation and methylation by the *O*-methyltransferase CysQ (Fig. 3A). The fragment C of **Cys 919-1** is synthesized by the same pathway, whereby β-hydroxy-L-Asn is isomerized to α-hydroxy-L-isoAsn by the aminomutase/amide dehydratase (AMDH) domain of CysH prior to methylation by CysQ yielding α-MeO-L-isoAsn. Also, L-Cya, an amino acid incorporated in low-abundant cystobactamid derivatives, is the product of the CysH AMDH domain. Deletion experiments of AMDH also showed that this domain is crucial for the *O*-methylation by CysQ, due to putative protein–protein interactions between AMDH and CysQ.[22] The detailed mechanism behind the dual functions of AMDH remains to be elucidated.

In the assembly of the full-length cystobactamid, three large NRPS genes *cysG*, *cysH* and *cysK* are involved. The assembly starts at the CysK NRPS, which loads and condensates the first two N-terminal *p*ABA units (Fig. 2). During or after peptide bond formation, the PABA-*N*-oxygenase CysR oxidizes the N-terminal amine yielding the terminal nitro functionality. CysB shuttles the central amino acid from CysH to NRPS-3 of CysK, where it is coupled with the N-terminal dipeptide, followed by the amide bond formation to the third *p*ABA unit (fragment D) at NRPS-4. The CysG NRPS loads unsubstituted and hydroxylated *p*ABAs, which are presumably synthesized by CysL and CysC. CysL is involved in the thioesterification of *p*ABA with Coenzyme A (CoA) (Fig. 5A), and the activated building block is oxidized to 3-hydroxy-*p*ABA-CoA and 2,3-dihydroxy-*p*ABA-CoA by CysC. The

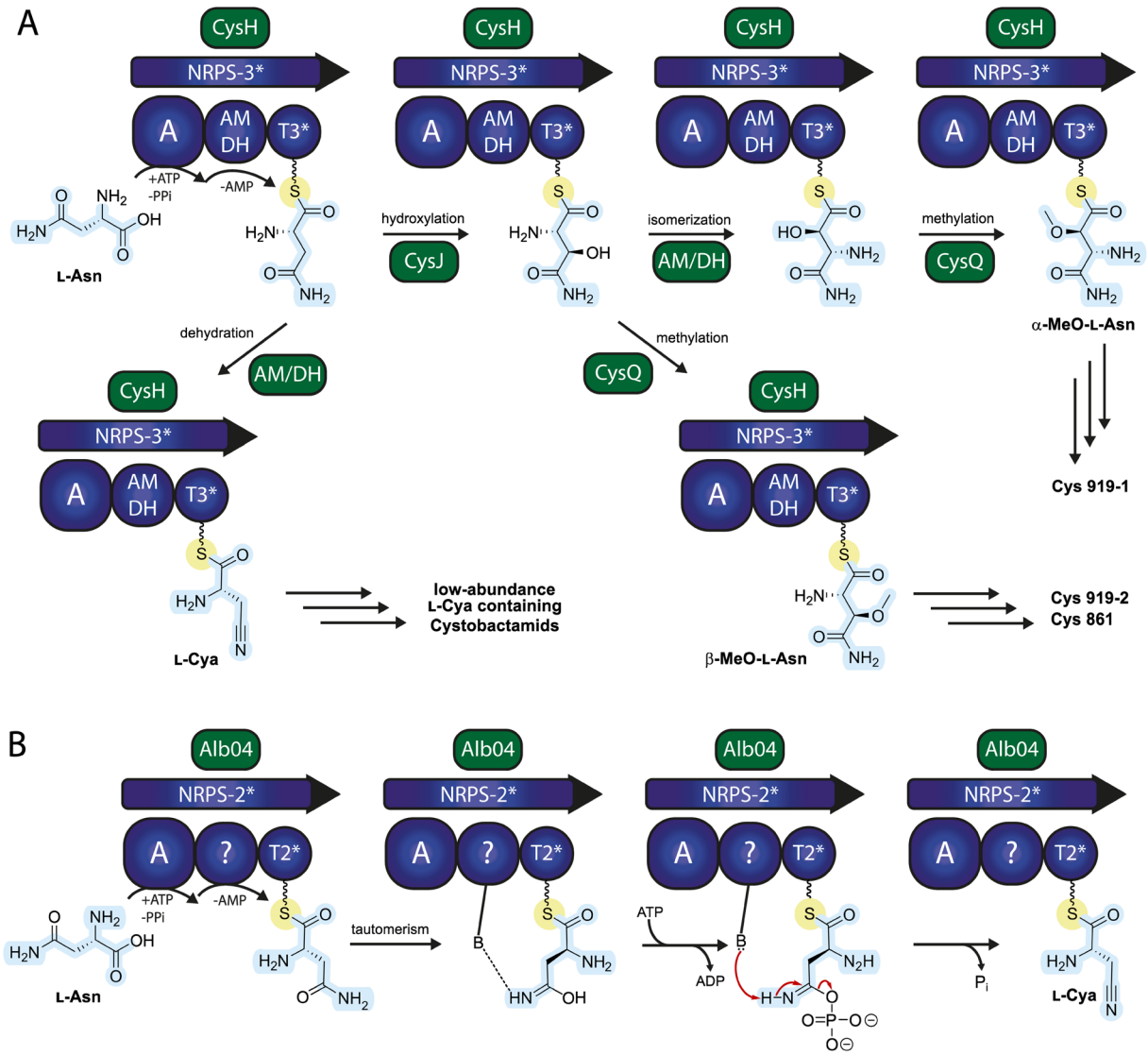


Fig. 3 Auxiliary NRPS synthesis of fragment C of cystobactamids and albicidin. (A) CysH activates and loads L-Asn and CysJ catalyzes the oxidation in β-position. Methylation by CysQ results in formation of β-MeO-L-Asn. Alternative pathways yield L-Cya or α-MeO-L-isoAsn by the action of the AM/DH domain of CysH. (B) Alb04 synthesizes L-Cya by dehydration of L-Asn.

SAM-dependent methyltransferase CysF acts as a tailoring enzyme for the alkylation of the 3-hydroxy group, followed by additional methylations by the cobalamin-dependent radical-SAM enzyme CysS (Fig. 5B) to give the characteristic isopropyl ether moieties of cystobactamids.[16] It is not entirely clear if the alkylating enzymes are acting on free *p*ABA-CoA or on loaded *p*ABA building blocks. The attachment of the *p*ABA building blocks of rings E and F, followed by TE-mediated product release, completes the biosynthesis of **Cys 919-2** or **Cys 861-2** (Fig. 2).

The gene locus encoding the biosynthesis of albicidins consists of 20 genes named *alb01* to *alb20* (Fig. 3B, 4, 5B and C). It encodes for an ADC synthase Alb17/pabAB and an ADC lyase Alb18/pabC to provide the required *p*ABA building blocks (Fig. 5C), similar to the cystobactamid biosynthesis.[14] Additionally, *alb20* encodes for a chorismate pyruvate-lyase-like protein (a 4-hydroxybenzoate synthetase) for the synthesis of 4-hydroxybenzoic acid. For the assembly, the three large NRPS genes *alb01*, *alb04* and *alb09* are essential (Fig. 4). In Alb01, a polyketide synthase modifies 4-hydroxybenzoic acid through a C2-extension, redox-reactions, dehydrogenation and a methylation, to obtain the MCA of fragment A, which is coupled with *p*ABA at NRPS-1. Subsequently, the incorporation of the central amino acid takes place with the help of a *trans*-acting NPRS-2* in Alb04. Alb04 shows specificity for L-Asn, which is dehydrated to L-Cya, with a postulated mechanism involving a phosphorylation of the amide oxygen, followed by phosphate elimination (Fig. 4B). Afterwards, the amide coupling with *p*ABA of fragment D is catalyzed by NRPS-3 (Fig. 4A). The precursors of the fragments E and F are synthesized by auxiliary NRPS domains. 3-Hydroxy-*p*ABA (*p*AHBA) is generated through an NADPH-dependent hydroxylation of *p*ABA by Alb12, a benzoyl-CoA oxygenase-like enzyme (Fig. 5C). After loading *p*AHBA to the $T_4$- or $T_5$-domain of Alb09, the methyltransferase Alb02 and the hydroxylase Alb08 transform *p*AHBA to the characteristic 3-methoxy-2-hydroxy-*p*ABA (*p*MBA) building block. Finally, the fragments E and F are incorporated by the modules NRPS-4 and NRPS-5 of Alb09 (Fig. 4A). The thioesterase domain of NRPS-5 mediates the release of albicidin. A low-abundance carbamoylated albicidin, formed by *O*-carbamoylation of the coumaric phenol by Alb15 post-NRPS, is a naturally occurring analogue (Fig. 4B). This ATP-dependent *O*-carbamoyltransferase catalyzes the activation of carbamoyl phosphate to form carbamoyl-AMP, which subsequently carbamoylates the MCA moiety of albicidin.

The structural distinctions between albicidin and cystobactamids primarily relate to the major components found in bacterial extracts. Upon closer examination of the minor components in both albicidin and cystobactamid producers, minor analogues that displayed structural characteristics associated with the respective 'other' class were identified. The cultivation of *Myxococcus* sp. SBCy9270, another producer of cystobactamids, led to eight novel analogues (Fig. 6A).

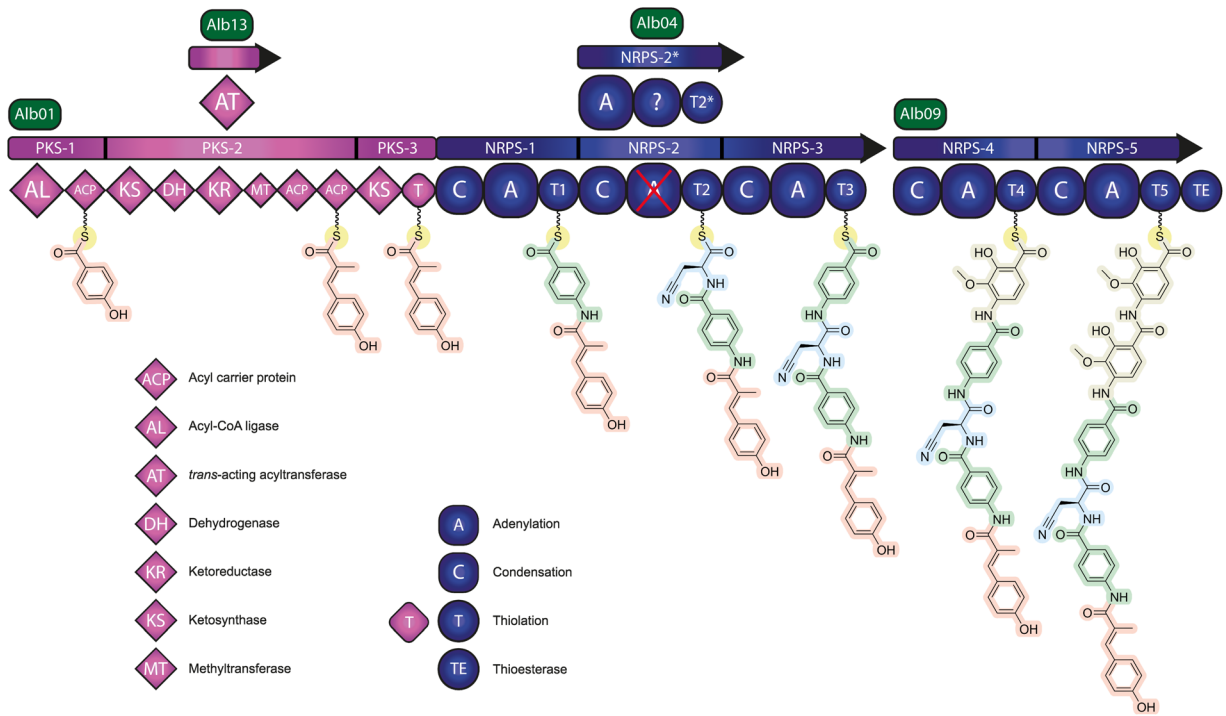


Fig. 4 (A) Model of albicidin biosynthesis. The PKS-NRPS hybrid assembly line is encoded by *alb01*, with the modules PKS-1–PKS-3 (purple) synthesizing MCA-1, and NRPS-1–NRPS-3 (blue arrow) incorporating *p*ABA-2, Cya-3 and *p*ABA-4. The *alb09* gene encodes modules NRPS-4 and NRPS-5, which install *p*MBA-5 and *p*MBA-6 (blue arrow). Synthesis of L-Cya, *p*ABA and *p*MBA is shown in Fig. 3 and 5. (B) Post-NRPS *O*-carbamoylation of albicidin. The ATP-dependent carbamoyltransferase Alb15 catalyzes the activation of carbamoyl phosphate, forming carbamoyl-AMP, which is subsequently transferred to the phenol moiety in fragment A of albicidin *via* acid–base catalysis, yielding carbamoyl–albicidin.

 

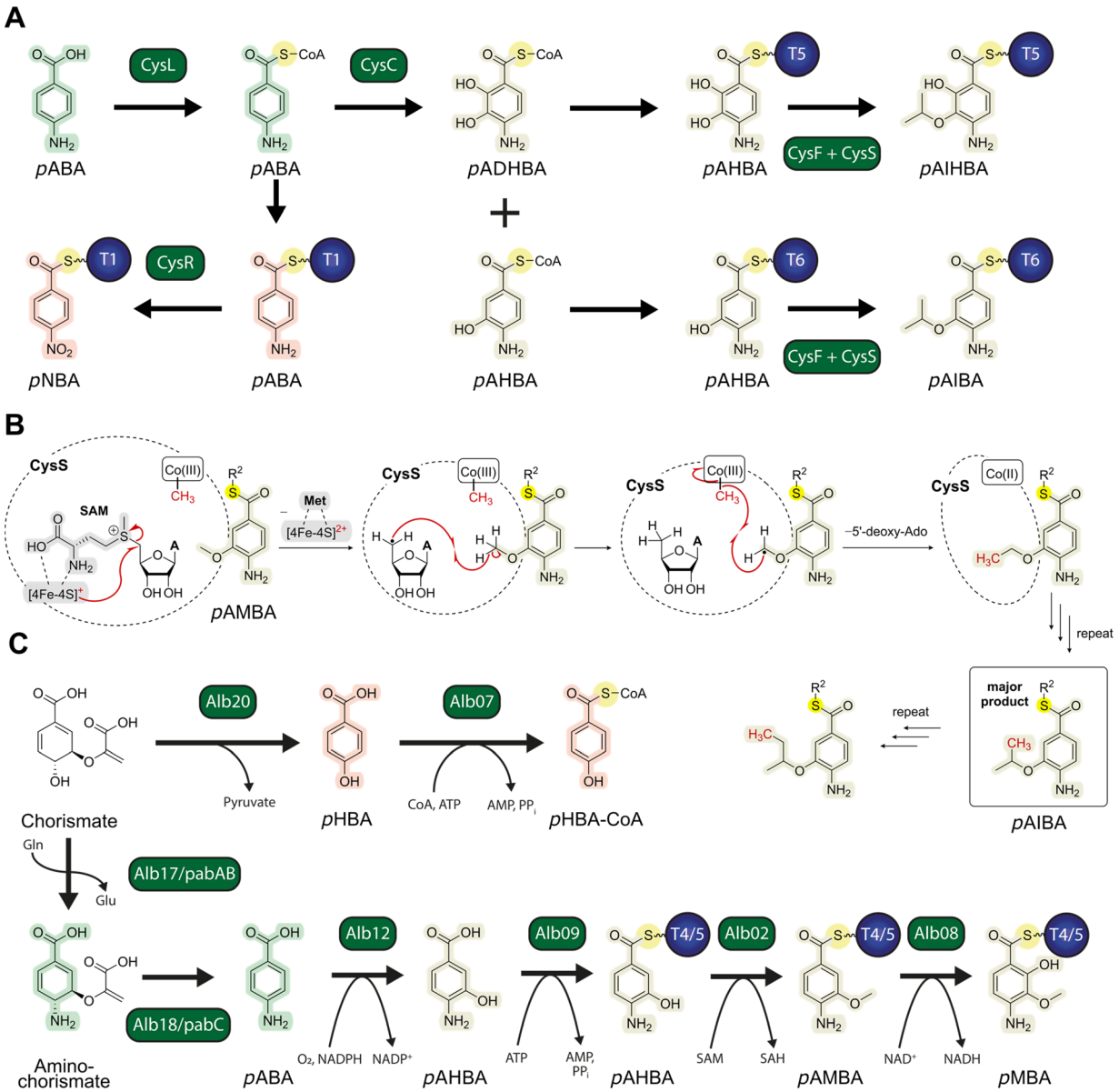


Fig. 5 Proposed biosynthetic pathways for *p*ABA precursors. (A) Cystobactamid related precursors are synthesized beginning with the thioesterification of *p*ABA by CysL. Fragment A is synthesized after loading to T1 and oxidation by CysR, yielding *p*NBA. CysC oxidizes *p*ABA-CoA to 2,3-dihydroxy-*p*ABA (*p*ADHBA)-CoA and 3-hydroxy-*p*ABA (*p*AHBA)-CoA. CysF loads *p*ADHBA or *p*AHBA, which are alkylated by CysS, yielding *para*-amino-2-isopropoxy-3-dihydroxybenzoic acid (*p*AIHBA) or *para*-amino-2-isopropoxybenzoic acid (*p*AIBA). (B) Proposed radical mechanism of the methylation of 4-amino-3-methoxybenzoic acid thioester (gold), catalyzed by CysS. The cobalamin complex [Co], the iron–sulfur cluster (4Fe–4S), and *S*-adenosylmethionine (SAM) are located in the active site of CysS, depicted as dotted circle. A = adenine, Ado = adenosine, $R^2$ = CoA or 4′-phosphopantetheine moiety of a T-domain. (C) Albicidin related precursors are synthesized from chorismate. Alb20 catalyzes the elimination of pyruvate, yielding the MCA precursor *para*-hydroxybenzoic acid (*p*HBA) of fragment A. Fragments B and D are synthesized by amination of chorismate followed by elimination of pyruvate, yielding *p*ABA. Fragments E and F are synthesized starting from *p*ABA, by oxidation catalysed by Alb12, loading to Alb09, methylation by SAM-dependent Alb02, and further oxidation by Alb08, producing *p*MBA.

Major differences between the cystobactamids were gathered at the central amino acid as well as the alkoxy substitution patterns at the *p*ABA of fragments E and F. Moreover, both β-MeO-L-Asp as well as β-MeO-L-isoAsp residues were found, in addition to the previously reported Asn analogues (Fig. 1). Notably, Cys 871, containing an L-Cya residue typically found in albicidins, as well as coralmycins A and B were also isolated, further highlighting the close structural relationship between coralmycins, cystobactamids and albicidins (Fig. 6A).[23]

Through heterologous production in *M. xanthus* DK1622 using an optimized expression vector system, 13 novel cystobactamids were produced, all representing natural derivatives composed of permutations of known structural elements. Furthermore, nine non-natural cystobactamids (Fig. 6A) were generated by targeted deletion of either *cysQ*, *cysJ*, the AMDH domain of *cysH*, *cysB* or *cysR* within the integrated expression vector, aiming to elucidate the functional roles of the corresponding NRPS genes. Most notable, the deletions led to the

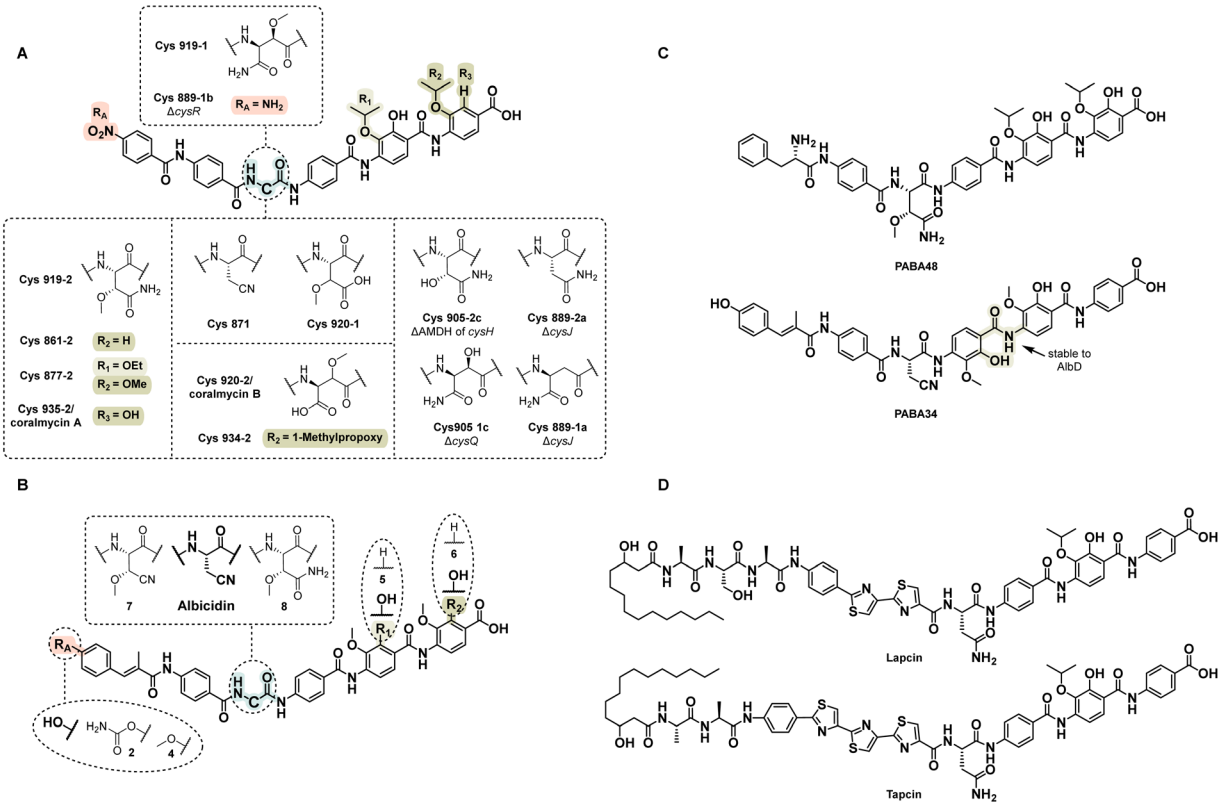


Fig. 6 Naturally occurring oligoarylamides. (A) Cystobactamids from Myxococcus sp. SBCy9270 and heterologously produced cystobactamid derivatives in *M. xanthus*, resulting from deletions in the introduced expression genome. (B) Natural analogues of albicidin. (C) Structures of PABA48 and PABA157. (D) Tapcin and lapcin.

incorporation of new asparagine derived linkers as well as analogues with an N-terminal amine instead of the nitro group.[22]

A comparison of their antibiotic activities revealed that derivatives containing asparagine-based amino acids were significantly more potent than aspartic acid analogs, consistent with earlier findings comparing coralmycin B to **Cys 919-2** (Fig. 6A and 1).[19] Of all isolated cystobactamids, **Cys 861-2** with an unsubstituted F-ring depicted the highest and broadest activity (Fig. 2). This was surprising, given that a higher oxidation and substitution appeared favorable in earlier analogs such as coralmycin A (Fig. 1). In conclusion, the superior potency of **Cys 861-2**, that formed the basis for subsequent chemical optimization efforts,[24] illustrated the value of an in-depth isolation effort even of minor components.[23,24]

By bioactivity-guided isolation and mass spectrometric networking, the structures of nine natural albicidin derivatives were predicted and confirmed by chemical synthesis (Fig. 6B).

Aside from the carbamoylated albicidin, none of the natural albicidin analogues demonstrated better antimicrobial activity than albicidin.[25,26] Modifications, including a β-methoxylated L-Cya and β-MeO-L-Asn, as well as dehydroxy variants of *p*MBA in the fragments E and F, were found with a remarkable similarity to the cystobactamid natural products.[22]

Screening soil metagenomes for *p*ABA-specific adenylation domain sequences by Wang *et al.* led to the identification of twelve biosynthetic gene clusters (BGCs) predicted to encode six novel congeners.[27] These synthetic bio-informatic natural products (*syn*-BNPs), comprising three cystobactamid and three albicidin derivatives were synthesized and exhibited differences in their activity spectrum. Among them, cystobactamid-derived PABA48 (Fig. 6C) with a phenylalanine as fragment A demonstrated the highest broad-spectrum antibiotic potency, while albicidin-derived PABA34 showed increased resistance to proteolytic cleavage by AlbD, likely due to its highly substituted fragment D.

Recently, Wang *et al.* utilized a combination of soil metagenome mining and bioinformatic tools to predict two related oligoarylamides with an unusual di-/tri-thiazole structure and an N-terminal lipopeptide moiety, which they named lapcin and tapcin (Fig. 6D).[28,29] Following the successful synthesis of these *syn*-BNPs, their biological characterization revealed a lack of antimicrobial or antifungal activity at the highest tested concentration (32 μg $mL^{-1}$). Instead of bacterial DNA gyrase ($IC_{50}$ > 20.5 μM for lapcin), human topoisomerases I and II were identified as their primary targets, with tapcin exhibiting $IC_{50}$ values of 203 nM and 71 nM, respectively. Furthermore, tapcin demonstrated potent antiproliferative activity against human cancer cell lines, with $IC_{50}$ values in the nanomolar to picomolar range, consistently outperforming the clinically approved topoisomerase inhibitors camptothecin and etoposide, although some toxicity against healthy cell lines was observed.

 

These potent *in vitro* effects translated into pronounced antitumor efficacy in both a mouse hollow fiber model and a xenograft model of colorectal adenocarcinoma (HT29 cells), with antiproliferative effects comparable to those of the clinically approved topoisomerase I inhibitor irinotecan.

The gene clusters for the synthesis of albicidins and cystobactamids express gene products with functional and structural similarity. Aside from the indispensable ability to synthesize the *p*ABA building blocks through *alb17*, *cysD* and *cysI*, both clusters contain three large analogue genes involved in connecting the fragments A–F: *alb01* and *cysK* for Fragment A–D, *alb04* and *cysH* for the activation and modification of fragment C and finally *alb09* and *cysG* for the attachment of fragment E and F.[14,15,22] Surprisingly, the stand-alone NRPS Alb04 and CysH show high sequence and structural similarity, yet different reaction mechanisms were proposed for both enzymes.[22] Due to the high structural similarity of fragment E and F, oxygenase and *O*-methyl transferase analogues can be found in both gene clusters, yet *cysS*, encoding for a radical-SAM *O*-methyl transferase, is exclusive for the cystobactamid gene cluster.[18] The differences in the gene cluster result in the unique structural features of both compound classes. This includes *alb20* and *alb07*, for the synthesis and loading of 4-hydroxybenzoic acid, the conversion of 4-hydroxybenzoic acid to MCA by the PKS subunit in Alb01 and *O*-carbamoylation facilitated by *alb*15.[14,25] In the cystobactamids gene cluster, *cysR* expression leads to *N*-oxidation to the nitro group, while the already mentioned *cysS* is responsible for the branched *O*-alkoxy at fragment E and F.[22]

# 3 Mechanism of action

## 3.1 Bacterial DNA gyrase as target

The elucidation of the mode of action (MoA) of any drug molecule is crucial for the rational design of analogs. In early work, the interference of albicidin with the DNA synthesis in *E. coli* was observed and gyrase determined as the target.[7] In the case of cystobactamids, the presence of pentapeptide repeat protein, associated with resistance to gyrase, within the biosynthetic gene cluster gave a hint to gyrase as a target.

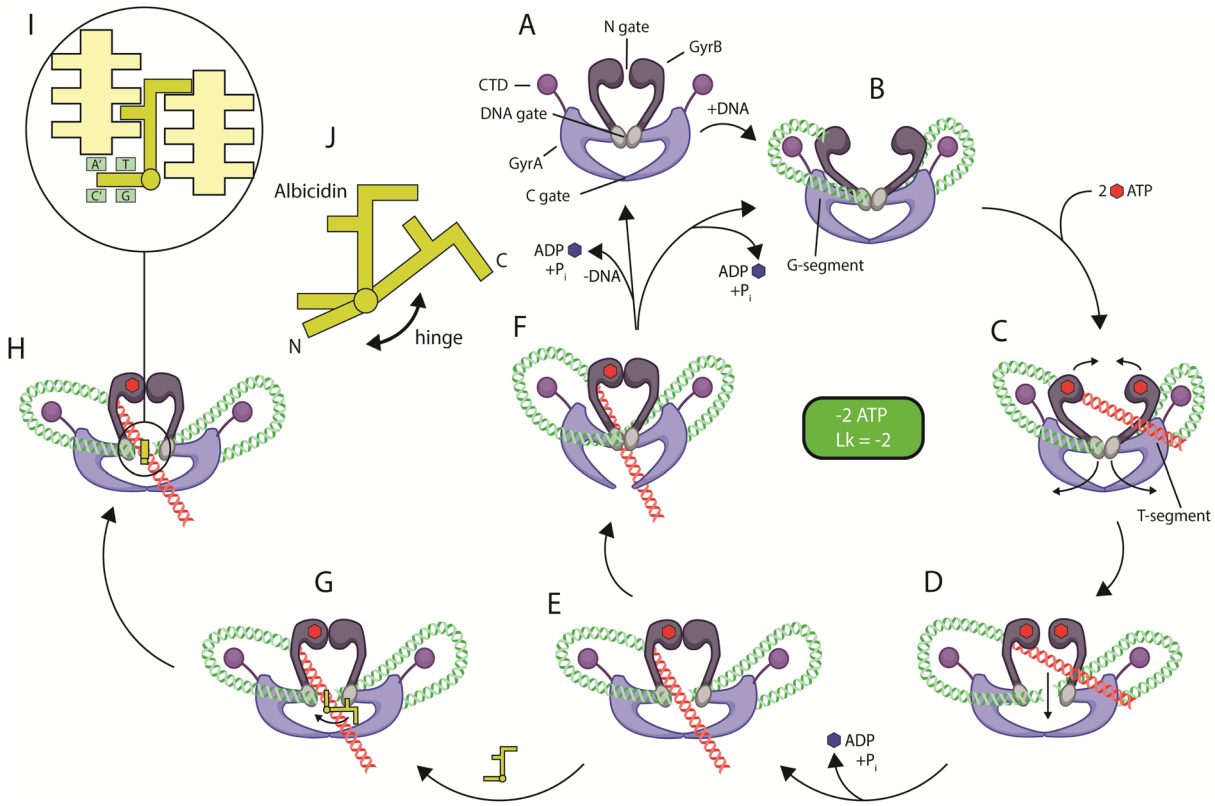


Fig. 7 Mechanism of the catalytic cycle of DNA gyrase. (A) Gyrase subunits GyrA (blue) and GyrB (dark violet) assemble into a heterotetrameric $A_2B_2$ complex. (B) The G-segment (green) binds to the DNA-gate. (C) DNA wrapping around the C-terminal domain (CTD, purple) positions the T-segment (red) perpendicular above the G-segment, followed by ATP (red hexagons) binding to GyrB and T-segment capture in the N-gate. (D) Cleavage of the G-segment, DNA-gate opening and passage of the T-segment through the N-gate are promoted by ATP hydrolysis, followed by dimerization of the ATPase domains. (E) Religation of the G-segment and closure of the DNA-gate are followed by transient opening of the C-gate and release of the T-segment. (F) Resetting of the enzyme for the next catalytic cycle by opening the N-gate is dependent on hydrolysis of the second ATP molecule. (G) Albicidin (yellow) initially intercalates into the cleaved DNA with its N-terminal fragment. (H) Before closure of the DNA-gate, the C-terminal fragment of albicidin rotates in between the GyrA/GyrA′ interface, thereby preventing religation of the DNA. (I) (Inset) Schematic representation of albicidin's binding mode. The N-terminal fragment of albicidin intercalates into the TG pocket and the C-terminal fragment binds to the α3/α3′ helices of the GyrA/GyrA′ interface. (J) Schematic structure of albicidin showing the hinge connecting its N- and C-terminal arms.

Ultimately, DNA gyrase and topoisomerase IV were confirmed as molecular targets of albicidin[12] as well as of cystobactamids through functional biochemical assays.[15] The bacterial topoisomerases are attractive antibacterial targets that are essential in bacteria and differ significantly in structure from their eukaryotic counterparts. The DNA gyrase alleviates torsional stress ahead of the replication fork by negatively supercoiling DNA. It operates as a heterotetrameric ($A_2B_2$) enzyme, composed of GyrA and GyrB subunits. Initially, a specific DNA sequence, known as the G (gate)-segment, binds to the DNA gate (GyrA/GyrA′ interface) while the adjacent DNA region is wrapped around the C-terminal domain (CTD) of GyrA (Fig. 7B), positioning the T (transfer)-segment above the G-segment. Consequently, a chiral wrap is formed with the T-segment positioned perpendicular to the G – segment (Fig. 7C).[30] Binding of two ATP molecules to the ATPase domain of GyrB is hypothesized to induce disengagement and undocking of the ATPase domain from the Toprim domain.[30] This leads to large conformational changes of the ATPase domain resulting in N-gate narrowing and capture of the T-segment (Fig. 7D).[30] The G-segment is cleaved through a transesterification reaction, where the phosphoryl group of the DNA strand reacts with the phenolic oxygens of active-site tyrosines (Tyr122 on GyrA/GyrA′- in *E. coli*) catalyzed by a GyrB-bound $Mg^{2+}$-ion. Cleavage of the double strand creates two scission sites between T/G and A/A with a four base pair overhang in between.[31] ATP hydrolysis on the ATPase domains promotes strand passage of the T-segment through the opened DNA gate (Fig. 7E).[32] This might be facilitated by the moving and rotating ATPase domains pushing the T-segment toward the lower cavity of the gyrase.[30] After strand passage, the space vacated by the T-segment enables dimerization of the ATPase domains.[30] Subsequently, the G-segment is re-ligated and the DNA gate closed (Fig. 7F).[33] Finally, the T-segment is released through the C-gate after which it closes and the enzyme is reset upon hydrolysis of a second ATP molecule.[34]

The ATPase function of gyrase is unaffected in presence of albicidin, whereas aminocoumarin antibiotics act as competitive inhibitors at the ATP binding site on GyrB.[12] MIC studies revealed a mild cross-resistance of fluoroquinolone-resistant *E. coli* strains to **Cys 919-1**, suggesting an overlapping but distinct binding site at GyrA.[15] In contrast to gyrase poisons from the

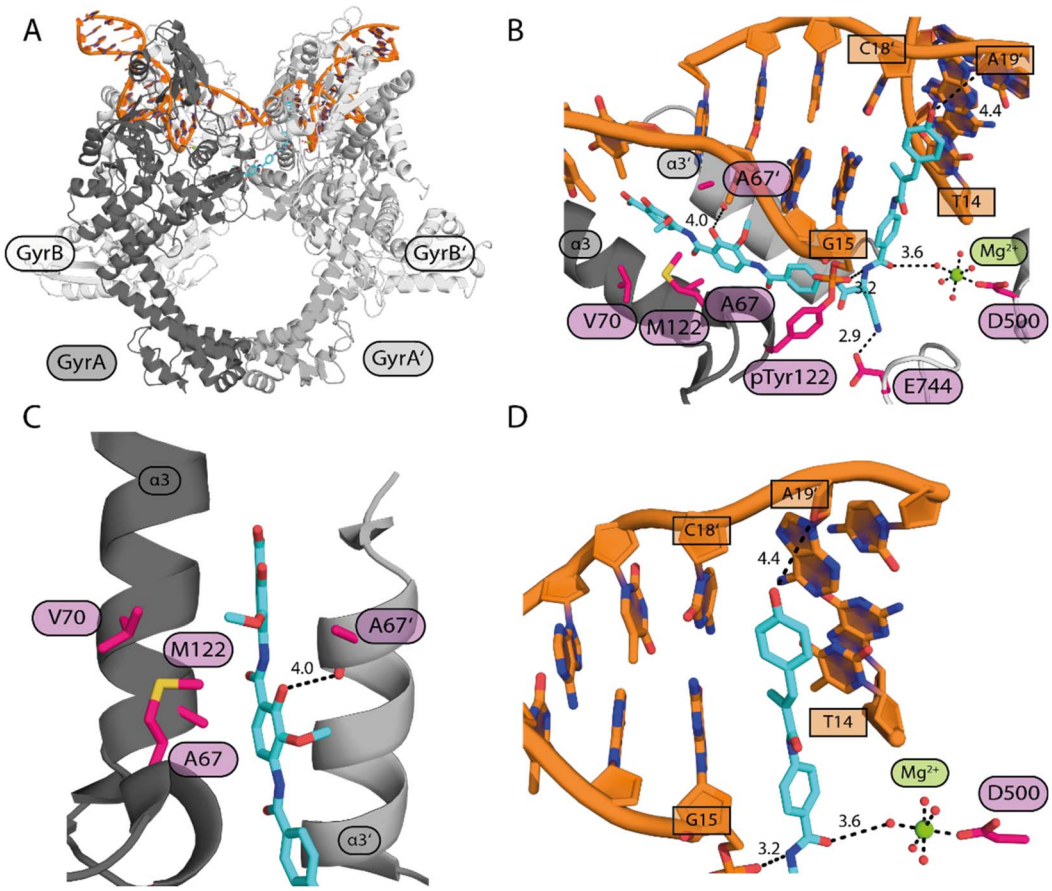


Fig. 8 Binding mode of albicidin to *E. coli* gyrase. Dashed lines represent hydrogen bonds. Bases G/A/T/C are shown in squared orange boxes, and amino acids in rounded pink boxes. Secondary structure elements are labelled with α (helix), and standard abbreviations are used for amino acids and bases. (A) Overview of gyrase with DNA (orange) and albicidin (cyan). GyrA (dark gray) and GyrA′ (medium gray), and both GyrB (light gray) subunits are displayed. (B) Overview of the albicidin binding pocket in gyrase. Residues interacting with albicidin (pink) and H-bonds (black dotted lines) with distances are highlighted. (C) GyrA/GyrA′ interface with the fragment DEF of albicidin in detail. Helices are labelled with their corresponding number. (D) T/G-binding pocket with the intercalating fragment AB of albicidin.

 

quinolone class, albicidin requires ATP for efficient stabilization of the cleavage complex of gyrase with DNA. This led to the hypothesis that albicidin binds to the DNA gyrase complex after strand passage (Fig. 7G).

### 3.2 Binding mode

The elucidation of albicidin's binding mode became feasible with advances in the field of cryogenic electron microscopy (cryo-EM). Identification of a suitable DNA fragment was the breakthrough in stabilizing the ternary DNA:gyrase:albicidin complex. A 217 bp DNA fragment from phage Mu (Mu217) was identified as an ideal gyrase substrate, promoting strong gyrase cleavage activity in the presence of albicidin. The structure of the inhibition complex revealed an asymmetric bicentric binding mode of albicidin to the gyrase tetramer (Fig. 8).[35] The DNA is cleaved at the scission sites 5′-**T**/**G**ATTT-3′ and 5′-**A**/**A**ATCA-3′ on the opposite strand.[31] The N-terminus of albicidin (MCA1 and *p*ABA2) intercalates into the T/G site, with MCA1 reaching C18′ and A19′ of the opposite strand (Fig. 8B and D). The amide bond between fragment B and C (*p*ABA2 and Cya3) interacts with the DNA-pTyr122 phosphodiester bond of the scission site and the water shell of the catalytic $Mg^{2+}$-ion. An H-bond is observed between the nitrile group of Cya3 and Glu744 on GyrB. The *C*-terminal end of albicidin (*p*MBA5 and *p*MBA6) is sandwiched between the α3/α3′ helices of the GyrA/GyrA′ interface, impeding the protomer movement that are crucial for relegation of the cleaved DNA. The methoxy groups of *p*MBA5 and *p*MBA6 occupy hydrophobic cavities on the α3/α3′ helices formed by the residues Ala67, Val70 and Met120 (Fig. 8C).

In this context, the binding modes of other albicidin/cystobactamid analogues were determined by cryo-EM. In contrast to the natural product, Albi-1 featuring a shortened fragment A (4-cyanobenzoic acid) was able to intercalate both the T/G site and the A/A site. Nevertheless, still only one ligand molecule is able to occupy either of the overlapping symmetric binding sites at a time. Furthermore, this analogue contained a L-azaHis in fragment C, which interacted with the water shell of the catalytic $Mg^{2+}$-ion and an isopropoxy group in fragment E that occupied the hydrophobic pocket at the α3/α3′ helices. A third binding mode with low occupancy was observed, in which the N-terminal segment of Albi-1 intercalated into the T/G site but showed no C-terminal interaction with the GyrA subunit interface (XT-state). This suggests that albicidin first intercalates into the DNA strand break with its N-terminus, leaving the C-terminus freely rotatable. Subsequently, the C-terminal arm of albicidin rotates between the GyrA/GyrA′ interface, preventing the closure of the DNA-gate. As a result, albicidin targets a transient conformation of the DNA gyrase following strand passage of the T-segment, effectively trapping the enzyme and causing replication stalling. Hence, the opening of the DNA gate is crucial for binding of albicidin to the GyrA/GyrA′-interface (Fig. 7G and H).[35] Notably, the solution conformation of cystobactamid CN-861 resembles the target-bound conformation of albicidin analogs. Thus, the conformational adaptation of the oligoarylamides upon gyrase binding incurs minimal energetic costs.[36]

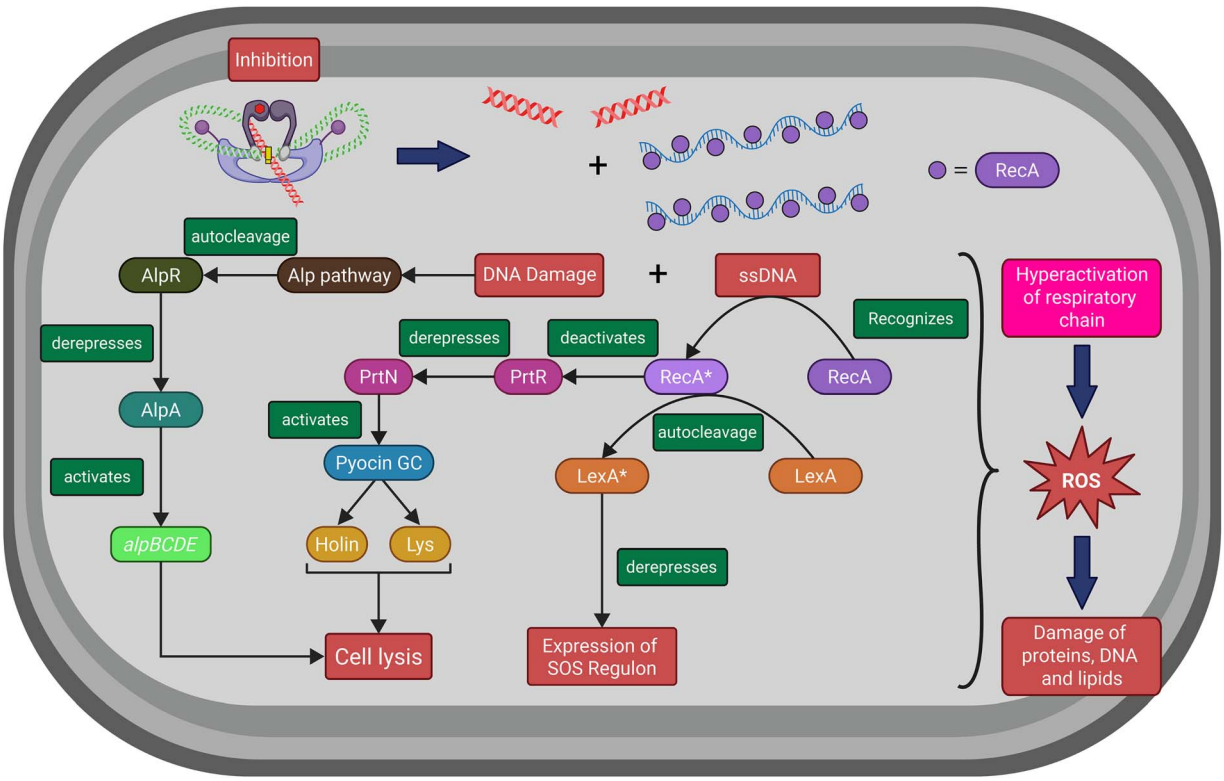


Fig. 9 Overview of transcriptomic effectors induced in *P. aeruginosa* upon treatment with cystobactamid. Enzymes are represented as round boxes, and effects are depicted as squares with rounded edges.

### 3.3 Cellular consequences of gyrase poisoning

To gain insight into the cellular consequences of gyrase inhibition by cystobactamid-type oligoarylamide antibiotics, the transcriptomic and metabolomic signatures induced in *P. aeruginosa* upon compound exposure at subinhibitory concentrations were analyzed. The signatures were compared to those induced by other classes, *i.e.* three GyrA-inhibiting fluoroquinolones and two aminocoumarins.[37] Notably, the three classes could be distinguished by transcriptomics as well as by metabolomics, although they all address the same target. The similarity of the GyrA-binding cystobactamids to fluoroquinolones was larger compared to the GyrB-binding aminocoumarins. Cystobactamids caused LexA-induced gene expression, indicating the presence of double strand breaks (DSBs) and a triggered SOS response (Fig. 9).[38]

In response to DNA damage, RecA controls several other pathways like the *lys* pathway, which contributes to programmed cell death. RecA facilitates the autocleavage of PrtR, which is a repressor of the *prtN* gene. The transcription activator PrtN regulates the R/F-pyocin region and activates the production of different bacteriocins (proteinaceous bacterial toxins).[39] As part of the pyocin gene cluster, the endolysin Lys (lytic bacteriophage protein)[40] and a putative holin protein[41] are co-expressed. Intracellular endolysin Lys is reported to degrade peptidoglycan following the permeabilization of the inner membrane by holins. A similar function has the Alp pathway controlled by the transcription regulator AlpR, which is functionally related to LexA. Autocleavage of AlpR derepresses *alpA* encoding for an antiterminator regulating the *alpBCDE* cell lysis genes.[37,42] The *lys* and the Alp pathway contribute to an altruistic suicide of the affected cell, whereby cellular components are ejected, enhancing virulence, biofilm formation and horizontal gene transfer.[40] Both pathways lys and Alp were upregulated in the presence of cystobactamids, ultimately resulting in suspected cell lysis. Additionally, the extent of endolysin induction coincided with the release of extracellular DNA.[37]

In conclusion, the cellular response to gyrase inhibition by oligoarylamide antibiotics is distinct from that of other gyrase inhibitors classes on a global-omics level. However, the major processes such as the induction of the SOS response resembles those induced by fluoroquinolones.

## 4 Mechanisms of resistance

### 4.1 Overview of resistance factors

Oligoarylamides are prone to bacterial resistance development, as is any antibiotic class. The understanding of bacterial resistance mechanisms is a prerequisite for attempts to bypass them or tone them down, as demonstrated by numerous preceding antibiotic classes.[43] A number of resistance factors counteracting the antibacterial effects of oligoarylamides have been identified and characterized on a molecular basis (Fig. 10). Resistance to them is believed to evolve in bacteria sharing

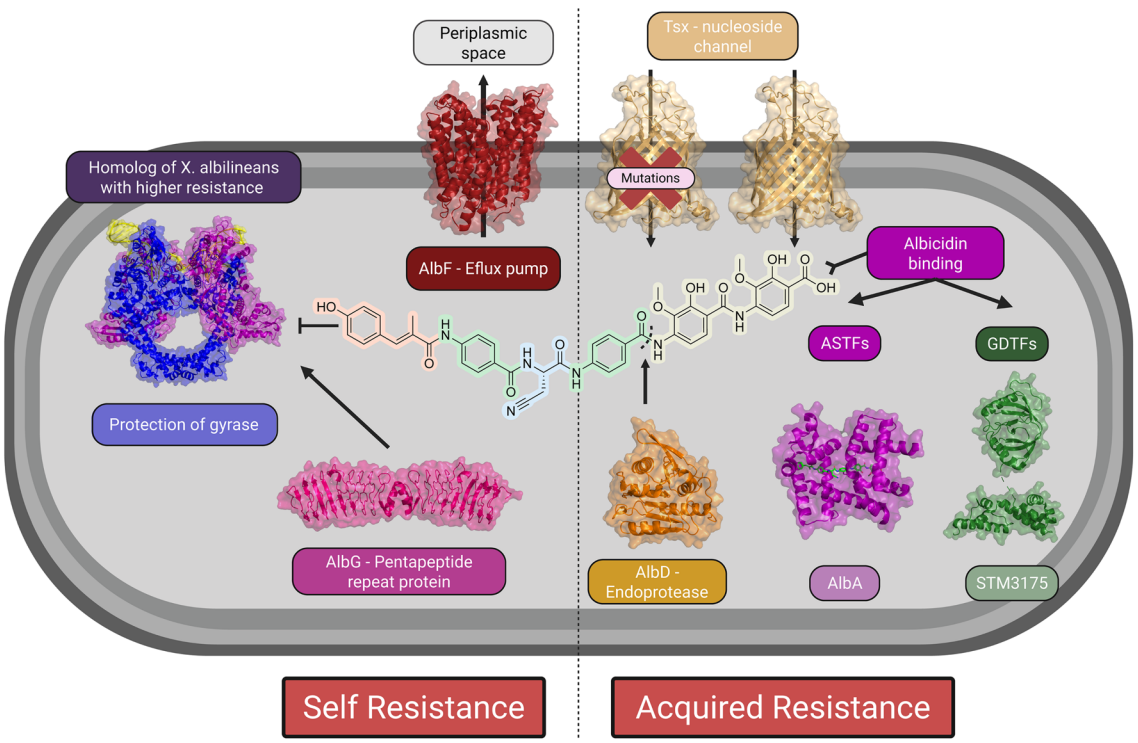


Fig. 10 A schematic representation of a Gram-negative bacterial cell highlighting known resistance mechanisms against the gyrase-poisoning effect of albicidin, with residue-specific colouring. Resistance mechanisms are categorized into self-resistance from *X. albilineans* (left) and acquired resistance in other bacteria (right). Proteinaceous resistance factors are shown in their tertiary structures with surface representation at 60% transparency. For clarity, the gyrase is represented schematically rather than in its quaternary structure. The structures of AlbD and AlbF were predicted using AlphaFold2.

 

a similar biotope with its natural producer, a process which is considered relevant for all natural antibiotic products.[44] In this context, mechanisms of self-resistance are imperative for bacteria producing secondary metabolites to avoid self-poisoning.[45] Usually, these self-resistance factors are tightly regulated and in most cases expressed simultaneously with the gene cluster for the biosynthesis of the antibiotic.[12,46,47] *X. albilineans* counteracts its own antibiotic by possessing the self-resistance proteins AlbF, AlbG and a modified gyrase. Additionally, known resistance mechanisms include albicidin sequestrating transcription factors (ASTFs),[48,49] gene duplication transcription factors (GDTFs)[50] and degrading enzymes.[51] Spontaneous resistance can also arise through mutation of uptake channels (Fig. 9).[52] Distribution of these defense mechanisms to other bacterial strains is possible *via* horizontal gene transfer (HGT).[53]

### 4.2 Gyrase from *Xanthomonas albilineans* and resistant mutants

An important line of defense against albicidin in *X. albilineans* is an altered gyrase homolog. Interestingly, this gyrase homolog also confers resistance to fluoroquinolones and coumarins, although less effectively than to albicidin. Bioinformatic analysis of the two gyrase subunits revealed two large insertions of 29 and 43 amino acids in the C-terminal region of the GyrA subunit, which play an important role in DNA wrapping and complex stability. In addition to these insertions, several amino acids in GyrA with a known involvement in enzyme activity or antibiotic resistance are altered.[12,54,55] An important amino acid in *E. coli* is Ser83 in GyrA, which is part of the quinolone-resistance determining region (QRDR).[56] This residue is indirectly involved in quinolone-gyrase interaction by mediating the drug binding through a non-catalytic $Mg^{2+}$ ion.[57] In *X. albilineans* this position is occupied by a glutamate (Q83) instead,[12] whereas in *E. coli* the GyrA mutants S83L/W/A confer resistance to fluoroquinolones. Additionally, the *E. coli* GyrA S83L mutant is slightly less susceptible to the natural product albicidin, resulting in a threefold decrease in gyrase activity.[35]

GyrB of *X. albilineans* differs from its *E. coli* homolog at two critical positions, which are involved in the catalytic function of the subunit. Concomitantly, these positions are associated with resistance to gyrase poisons in *E. coli*. The residues Q151 and R463 in the GyrB of *X. albilineans* correspond to R136 and K447 in wild-type *E. coli*.[58] The mutant $GyrB^{K447W}$ showed decreased sensitivity to FQs,[59] whereas the mutations R136C/H/L/S were identified in the GyrB of coumarin resistant *E. coli* strains.[60]

To date, no gyrase mutations causing albicidin resistance have been reported in directed evolution experiments. Nevertheless, resistance of other gyrase mutants against albicidin were evaluated. The $GyrB^{K447W}$ variant from FQR *E. coli* gyrase was less susceptible to albicidin, resulting in a 10-fold increase in $CC_{50}$. Mutations at the $\alpha3/\alpha3'$ interface of GyrA, where albicidin's alkyloxy substituents in fragment EF interact, also resulted in reduced albicidin sensitivity. The $GyrA^{A67Q}$ variant has a smaller and more polar pocket, which impaired hydrophobic interactions and led to a 13-fold increase in $CC_{50}$. Moreover, an increased size of the hydrophobic pocket as in the $GyrA^{V70A}$ variant further reduces the target activity (27-fold $CC_{50}$ increase), as hydrophobic interactions are hampered.[35] Notably, improved synthetic albicidin derivatives restored target activity against the majority of these mutants.

### 4.3 AlbG – pentapeptide repeat protein

*X. albilineans* produces AlbG, a pentapeptide repeat protein (PRP),[61] that prevents gyrase inhibition.[12] A similar PRP, CysO, was found in *Cystobacter* sp. and likely serves a similar function.[15] The crystal structure of AlbG[62] revealed high structural similarity to other PRPs that counteract gyrase poisons, including fluoroquinolones (MfpA[63] from *M. tuberculosis*, QnrB1 (ref. 64) from *K. pneumoniae*) or microcin B17 (McbG from *E. coli*). AlbG is highly effective in protecting *E. coli* against albicidin. This resulted in a more than 128-fold increased MIC against transformed *E. coli* cells harboring the *albG*-gene in comparison to the WT strain.[65] In general, PRPs confer protection against gyrase poisons. For the PRP QnrB1, two mechanisms were proposed: PRP binding to gyrase reduces the likelihood of antibiotic binding to it. Alternatively, PRPs may bind to the stabilized cleavage complex of the bound antibiotic and induce structural changes of the complex that result in the dissociation of the toxin and gyrase rescue.[65] Due to the structural similarity between QnrB1 and other PRPs, similar mechanisms are likely for AlbG or CysO.

### 4.4 AlbF – albicidin efflux pump

A widespread strategy of self-resistance against antibiotics with cytoplasmic targets involves the active removal of the poison from the cytoplasm *via* efflux mechanisms.[66] In *X. albilineans*, the efflux pump AlbF is located in the cytoplasmic membrane. This membrane protein belongs to the major facilitator family,[67] showing high sequence similarity to efflux proteins from antibiotic-producing actinomycetes.[68,69] Controlled expression of AlbF in *E. coli* resulted in a 3000-fold increase of resistance against albicidin, but not to other antibiotics, indicating that AlbF is highly specific for albicidin.[47]

### 4.5 AlbA/B – albicidin sequestrating transcription factors

The albicidin sequestrating transcription factors (ASTFs) represent the largest class of known resistance factors against albicidin. Among the characterized ASTFs are AlbA (*Klebsiella oxytoca*)[49] and AlbB (*Alcaligenes xylosoxidans*),[48] which both belong to the MerR-like transcription factor (TF) family. Typically, these TFs consist of a DNA-binding domain (DBD), a coiled-coil dimerization interface and a ligand binding domain (LBD).[70–72] MerR-like TFs function as stress sensors, detecting environmental stressors and regulating transcription activation as part of stress response.[73] AlbAL, the full length version of the TF, exists as a dimer in solution and binds with high affinity to the promoter *pAlbA via* both DBDs. Similar to other MerR-like TFs, AlbAL acts as repressor in the absence of a suitable ligand. Upon cell entry and recognition of albicidin by the LBD of AlbAL, allosterically mediated DNA-bending *via* the pair of DBDs is hypothesized.[74,75] The activated promoter

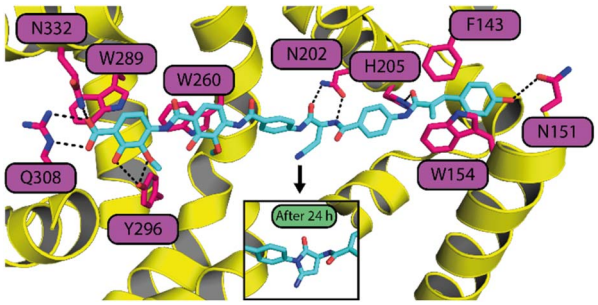


Fig. 11 Close-up view of the albicidin (cyan) binding pocket in AlbAS (yellow, PDB: 6ET8). AlbAS is depicted in cartoon and residues interacting with albicidin are highlighted pink. Hydrogen bonds are indicated by dotted blue lines. Cyclization of cyanoalanine to a succinimide after 24 hours is displayed in the black box (PDB: 6H96).

enables recruitment of RNA-polymerase, facilitating the transcription of AlbAL and the short gene product AlbAS featuring only the LBD.[49] The latter is predominantly responsible for sequestration of albicidin, thereby protecting DNA gyrase from inhibition.[76]

The crystal structure of the albicidin-AlbAS complex revealed an exclusively α-helical, pseudodimeric fold.[76,77] AlbA binds fragment ABC of albicidin with the N-terminal domain (NTD) and fragment DEF with the C-terminal domain (CTD). Several amino acids work in concert to trap albicidin with nanomolar affinity ($K_d$ = 5.6 nM). The hydrophobic binding pocket is primarily shaped by aromatic amino acids which engage in π–π stacking interactions with albicidin (F143, W154, W260, W289). Several H-bond interactions (Asn151, His205, Asn202, Tyr296, Gln332) and a salt bridge (R181) hold the molecule in place (see Fig. 11).[76]

In addition, cyclization of the central L-Cya moiety of albicidin, catalyzed by AlbA, was reported to yield a less active succinimide derivative.[77] In the course of SAR studies, this inactivation mechanism could be avoided by replacing Cya with chemically inert amino acids, such as L-azaHis, that retained biological activity.[13,78]

Mutational studies with AlbAL in combination with a reporter assay, utilizing the *ilux* luminescence cassette, identified P209, W289 and Y296 as critical residues for the ability to mediate transcription activation.[74] Furthermore, no correlation between high affinity binding of albicidin and the ability to trigger transcription activation was observed. Understanding of the stimulus transmission from the LBD to DBD requires further study.

### 4.6 STM3175/YgiV – oligoarylamide binding proteins

Spontaneous resistance against albicidin in *Salmonella enterica* serovar Typhimurium (*S.* Typhimurium) arises through gene duplication and amplification for STM3175 (YgiV in *E. coli*).[50] The gene duplication–amplification (GDA) mechanism involves duplications of genomic regions, causing increased gene copy numbers resulting in higher gene product dosages.[79] These gene duplications allow bacteria to rapidly adapt to selective pressures and are frequently associated with the emergence of antibiotic resistance.[80]

The transcription factor STM3175 was discovered after serial passaging of *S. Typhimirium* with albicidin to generate high-level resistance mutants, which gained up to 15 copies of the gene. STM3175 adopts a structural fold distinct from AlbA and consists of a LBD with sub-micromolar affinity for albicidin ($K_d$ = 0.17 μM), as well as a DBD of unknown function.[50] Molecular docking studies suggested binding of albicidin into a groove in the center of the LBD in a 1 : 1 stoichiometry. Intriguingly, overexpression of the full-length protein led to higher resistance than the LBD alone, although both exhibit similar affinities for albicidin. Hence, STM3175 may employ an additional, yet unidentified resistance mechanism beyond albicidin sequestration. A potential association between GDAs and efflux pumps appears unlikely, as single-gene knockouts of all known efflux systems in *S.* Typhimirium had no effect on albicidin susceptibility.[81]

For cystobactamids, resistant *E. coli* mutants had single nucleotide polymorphisms in the promotor region of the ygiV gene that led to strongly upregulated protein levels. YgiV bound the cystobactamid CN-861-2 with high affinity ($K_d$ = 0.036 μM), but also led to a reduced expression of virulence factors.[82]

### 4.7 AlbD – endoprotease

The serine endopeptidase AlbD from *Pantoea dispersa* was found to catalyze the hydrolysis of albicidin between the fragments D and E.[83–85] Since the resulting fragments lack antibacterial activity, AlbD detoxifies albicidin, conferring protection to the bacterial cell. Expression of the *albD* gene in *E. coli* conveyed resistance against albicidin.[86] The minimal cleavage motif of AlbD, elucidated from synthetic derivatives, consists of tripeptides with a H-DEF-OH or Ac-CDE-OH core motif.[85] AlbD also degrades cystobactamids and DEF fragments featuring isopropoxy ethers, although with slightly lower cleavage efficiency.[24,85]

### 4.8 Tsx – albicidin uptake channel

The nucleoside transporter Tsx is an outer membrane protein of Gram-negative bacteria and belongs to the porin family.[87] This channel appears ubiquitous among Gram-negative bacteria, with homologues identified in *E. coli*, *S.* Typhimurium, *K. pneumoniae* and *E. aerogenes* and has been implicated as an entry point for albicidin.[52,88] Resistance to albicidin was reported in *tsx* knockout mutants,[52] as well as in strains harboring point mutations or a 39-bp duplication. The point mutations primarily affect amino acids located in the outer loop region, which is putatively involved in substrate recognition, and within the pore formed by Tsx.[89] The reduced ability to import nucleosides into the cell also negatively impacts albicidin uptake, suggesting a shared entry or recognition mechanism.[89,90]

Notably, albicidin uptake-deficient mutants have emerged under conditions in which Tsx is dispensable. However, under carbon starvation conditions, relevant in infection scenarios, *E. coli* relies on Tsx-mediated nucleoside uptake.[91–93] Thus, reduced

 

Tsx function imposes fitness costs and is not readily tolerated under such conditions.

## 5 Total synthesis of oligoarylamides

The total synthesis of albicidin was achieved through a highly convergent strategy.[94] The molecule was strategically divided into three fragments at the cutting points I and II (Fig. 12A). Fragment **A** was introduced in the last step, due to limited solubility upon introduction of the coumaric acid into the peptide chain. Thus, the synthesis and the amide coupling of the fragments **BCD** and **EF** was conducted first. The low nucleophilicity of the anilines required rigorous reaction conditions *via* the activation of the benzoic acids as acid chlorides, which was achieved using triphosgene (BTC) as a coupling agent. Consequently, a robust protection strategy was necessary to protect the hydroxy and carboxy functions in fragments **A**, **E** and **F**. The allyl group proved stable under various reaction conditions employed during the synthesis. Its installation was facile, while global deprotection could be achieved under mild conditions. The assembly of the tripeptide **BCD** started with the formation of dipeptide **CD** from Boc-protected Asn (**C**) and *tert*-butyl amino benzoate H-*p*ABA-O*t*Bu (**D**) employing DCC as coupling agent. This facilitated amide bond formation and the dehydration reaction in one pot in good yields. The resulting dipeptide **3** was deprotected in presence of HCl in dioxane and coupled with preactivated aniline-masking $NO_2$-*p*ABA-OSu, giving tripeptide **BCD**. The key fragments **E** and **F** were synthesized starting from *ortho*-vanillin (**1**), which was *O*-acetylated to direct the following nitration to the *para*-position of the aldehyde function.[95,96] After hydrolysis, the phenol in **2** was re-protected with the allyl-group, and the aldehyde function was oxidized by a Pinnick oxidation giving fragment **E**. The synthesis of fragment **F** was accomplished by the allylation of the carboxylic acid in fragment **E** and reduction of the nitro-group using $SnCl_2$. Subsequently, both fragments were coupled using the BTC protocol, and the nitro-group of the resulting dipeptide was reduced to the corresponding aniline, giving fragment **EF**. The BTC coupling of the fragments **BCD** and **EF**, followed by nitro reduction, allowed the formation of the pentapeptide **BCDEF**. The final coupling with the allyl protected fragment **A** and the global allyl deprotection afforded the natural product albicidin with an overall yield of 6%.

Many aspects of the pioneering albicidin synthesis, such as the A + BCD + EF coupling strategy, the utilization of the allyl protection group and the chlorination agents in amidation reactions, were employed in subsequent syntheses of oligoarylamide containing natural products.[26–29,97,98]

For the unusual α-amino acid (2*S*,3*R*)-β-methoxy-asparagine, initially discovered in cystobactamids, three synthetic routes were independently reported (Fig. 13).

Route 1 (target: **Cys 861-2**)[23,99] employed stereoselective sharpless asymmetric dihydroxylation of methyl cinnamate (**3**), later followed by nucleophilic ring opening of sulfite **5** with

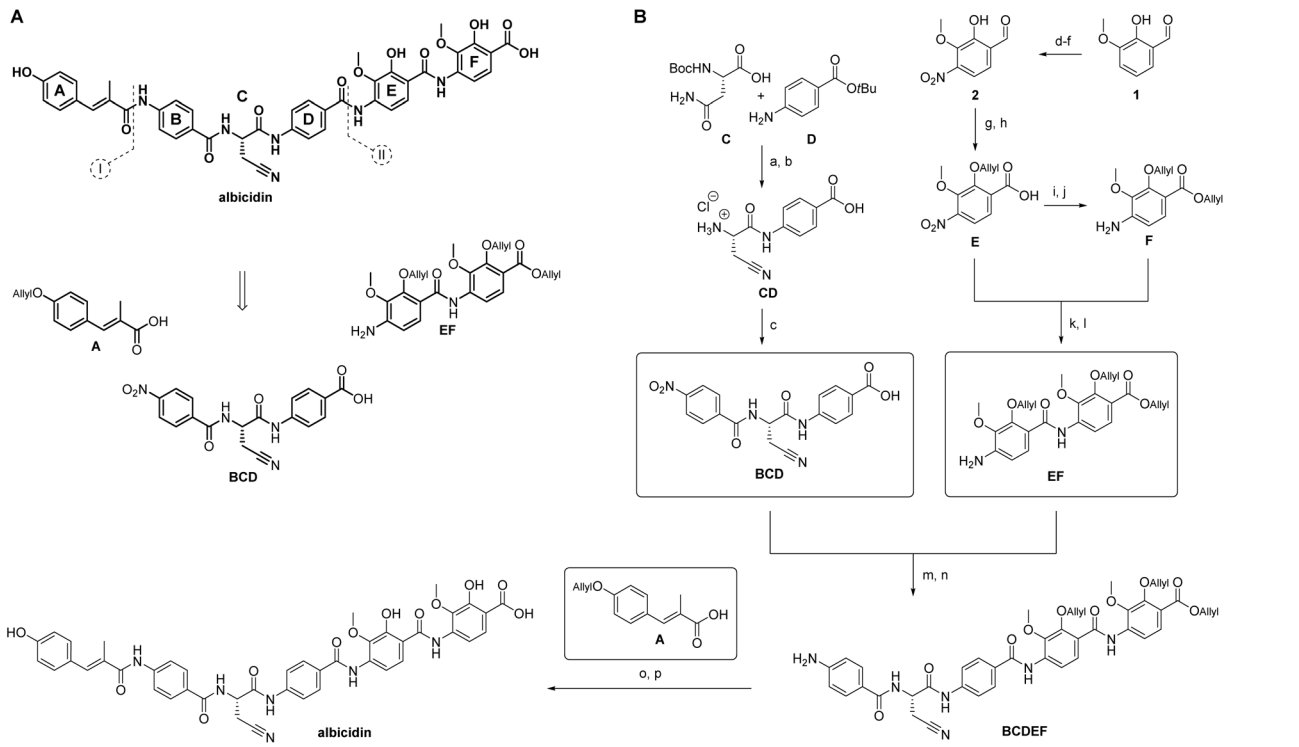


Fig. 12 (A) Retrosynthesis of albicidin, showing the coupling sites I and II, giving the three fragments **A**, **BCD** and **EF**. (B) Total synthesis of albicidin. Key intermediates **A**, **BCD** and **EF** are in boxes.[94] Reagents and yields: (a) DCC, 64%, ee 96%; (b) HCl (4 M), quant.; (c) $O_2N$-*p*ABA-OSu, $NEt_3$, 89%; (d) $(CH_3CO)_2O$, pyridine, 97%; (e) $HNO_3$, $H_2SO_4$; (f) NaOH, 73% for 2 steps; (g) allyl bromide, $K_2CO_3$, 88%; (h) $NaClO_2$, $NaH_2PO_4$, 2-methyl-2-butene, *t*BuOH, 92%; (i) allyl bromide, $K_2CO_3$; 93%; (j) $SnCl_2 \cdot 2H_2O$, 86%; (k) BTC, 2,4,6-collidine, DIPEA, 91%; (l) $SnCl_2 \cdot 2H_2O$, 79%; (m) BTC, 2,4,6-collidine, DIPEA, 91%; (n) $SnCl_2 \cdot 2H_2O$, 73%; (o) BTC, 2,4,6-collidine, DIPEA, quant.; (p) $Pd(PPh_3)_4$, phenylsilane, 26%.

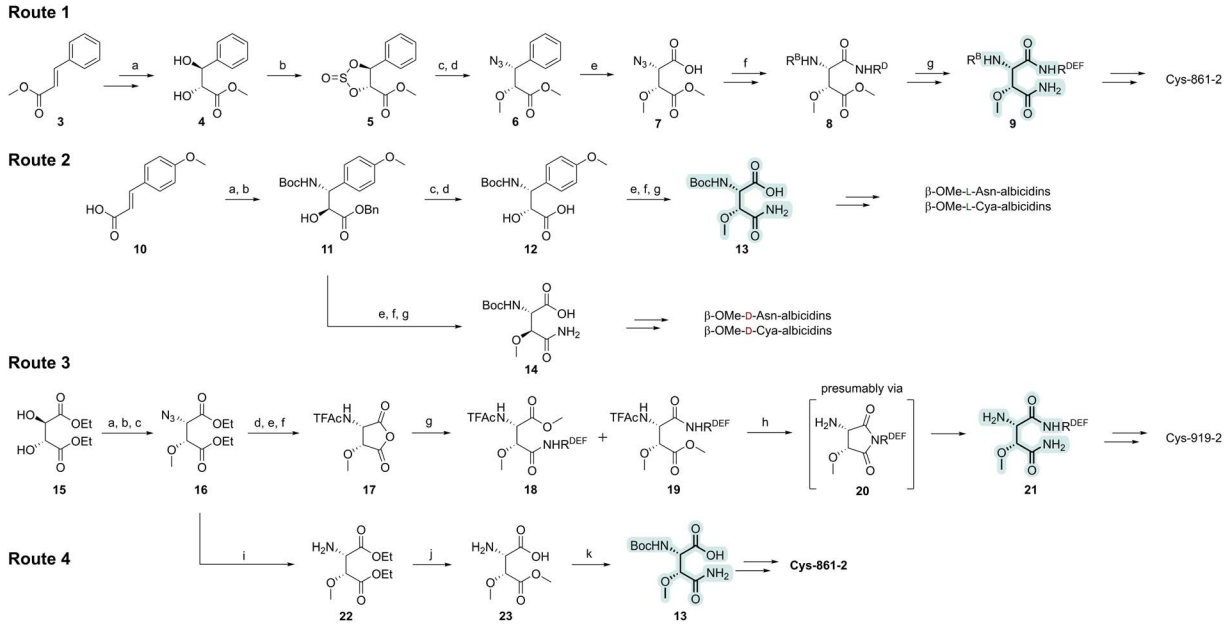


Fig. 13 Comparison of synthetic strategies for β-OMe-L-Asn used in the synthesis of different oligoarylamide antibiotic s. Reagents and yields. Route 1: (a) $(DHQ)_2PHAL$, $K_2[OsO_2(OH)_4]$, NMO (60% in water), 72%, ee 99%; (b) $SOCl_2$, 98%; (c) (1) $NaN_3$, (2) $H_2O$, 61%; (d) $CH_3I$, $Ag_2O$, $CaSO_4$, 85%; (e) (1) $RuCl_3$, $NaIO_4$, 71%, (2) $POCl_3$, *tert*-butyl 4-aminobenzoate, DIPEA, 81%; (f) (1) $PPh_3$, $H_2O$, (2) 4-nitrobenzoyl chloride, DIPEA, 71% for 2 steps; (g) 7 N $NH_3$ in MeOH, 51%. Route 2: (a) oxalyl chloride, then BnOH, pyridine, 92%; (b) *t*BuOCONH$_2$, *t*BuOCl, $(DHQD)_2PHAL$, $K_2[OsO_2(OH)_4]$, NaOH, 85%, ee 99%; (c) *para*-nitrobenzoic acid, $PPh_3$, DEAD; (d) $NaN_3$, MeOH, 85% for 2 steps; (e) $CH_3I$, $Ag_2O$, 92–93%; (f) $H_2$, Pd/C, 93–96%; (g) $Boc_2O$, $NH_4HCO_3$, pyridine; 79–83%; (h) $RuCl_3$, $NaIO_4$, 52–55%. Route 3: (a) $SOCl_2$, quant.; (b) (1) $NaN_3$, (2) $H_2O$, 70–80%; (c) $CH_3I$, $Ag_2O$, 99%; (d) $H_2$, Pd/C, 91%; (e) HCl (6 M); (f) TFAA, quant. for 2 steps; (g) $HC(OCH_3)_3$, 69%; (h) $NH_3$ (aq.), 60%. Route 4: (i) $H_2$, $Pd(OH)_2$/C, EtOAc, 97%; (j) (1) HCl/$H_2O$, (2) propylene oxide, (3) AcCl, MeOH, 55% over 3 steps; (k) (1) $Boc_2O$, $NaHCO_3$, (2) $NH_3$, 90% for 2 steps.

azide to introduce the amino nitrogen in intermediate **6**. After stepwise integration of the α-amino acid into the cystobactamid backbone, the primary amide of β-OMe-Asn was installed at the BCDEF fragment stage **9** *via* aminolysis of the methyl ester.

In route 2 (target: β-OMe-Asn/β-OMe-Cya containing albicidins),[26] methoxy cinnamic acid (**10**) underwent aminohydroxylation to give Boc-protected amino alcohol **11**, followed by inversion of the alcohol *via* a Mitsunobu reaction. With alcohols **11** and **12** available, access to β-OMe-Asn was enabled *via* methylation, benzyl ester deprotection, primary amide formation, and oxidative degradation of the aromatic ring, affording Boc-β-OMe-L-Asn (**13**) and Boc-β-OMe-D-Asn (**14**).

In route 3 (target: **Cys 919-2**),[98,100] similar to the diol **4** in route 1, L-diethyl tartrate (**15**) was converted into a the 2-methoxy-3-azido substituted diester **16** which was reduced and cyclized yielding anhydride **17**. Aminolysis of cyclic anhydride **17** incorporated the fragment C precursor into the cystobactamid backbone, followed by isomerization. This presumably involved the cyclic aspartimide intermediate **20** to yield β-MeO-Asn **21** on the CDEF fragment stage. Scalability was achieved with route 4 (target: **Cys 861-2**),[101] starting with double ester hydrolysis of intermediate **22**, followed by selective methylation of the β-carboxylic acid. Subsequent aminolysis of methyl ester **23** with ammonia yielded Boc-β-MeO-Asn (**13**).

For the first total synthesis of cystobactamid 861-2 (Fig. 14A), the A + BCD + EF coupling strategy (Fig. 12A) was utilized. The central BCD-tripeptide **8** was built after unmasking of the carboxylic acid of key building block **6** and coupling to H-*p*ABA-O*t*Bu using $POCl_3$, followed by coupling of 4-nitrobenzoyl chloride to the liberated amine of the CD-dipeptide **24**. The synthesis of fragment **EF** started from dihydroxybenzaldehyde **25**. The isopropoxy ether was introduced by regioselective alkylation of the *meta*-hydroxy group followed by acetylation of the *ortho*-hydroxy group. Regioselective nitration resulted in formation of the tetrasubstituted benzene **26**. The acetyl group was replaced by an allyl group and the aldehyde was subjected to a Pinnick oxidation, yielding key intermediate **27**. Fragment EF was formed by a $POCl_3$ mediated coupling of carboxylic acid **27** with H-*p*ABA-OAllyl, and reduction of the nitro group resulted in formation of amine **28**. The endgame of the synthesis involved $POCl_3$ mediated coupling of the BCD-tripeptide **8** and **EF** dipeptide **28** and nitro reduction yielding BCDEF-pentapeptide **9**, which was coupled to 4-nitrobenzoyl chloride. Global allyl-deprotection resulted in the formation of **Cys 861-2**. A more recent synthesis[101] assembles cystobactamid 861-2 by an AB + C + DEF strategy, which was also used in the synthesis of β-OMe-Asn-albicidin (Fig. 14B), whereby the final coupling takes place between the fragments AB and CDEF. This retrosynthetic approach was most frequently utilized in the synthesis during the development of new cystobactamid and albicidin analogues by medicinal chemistry.[13,78,102–107]

Because of their higher antibiotic potency, synthetic efforts were focused on oligoarylamides with an α-amino acid in position C. However, a total synthesis of the natural

 

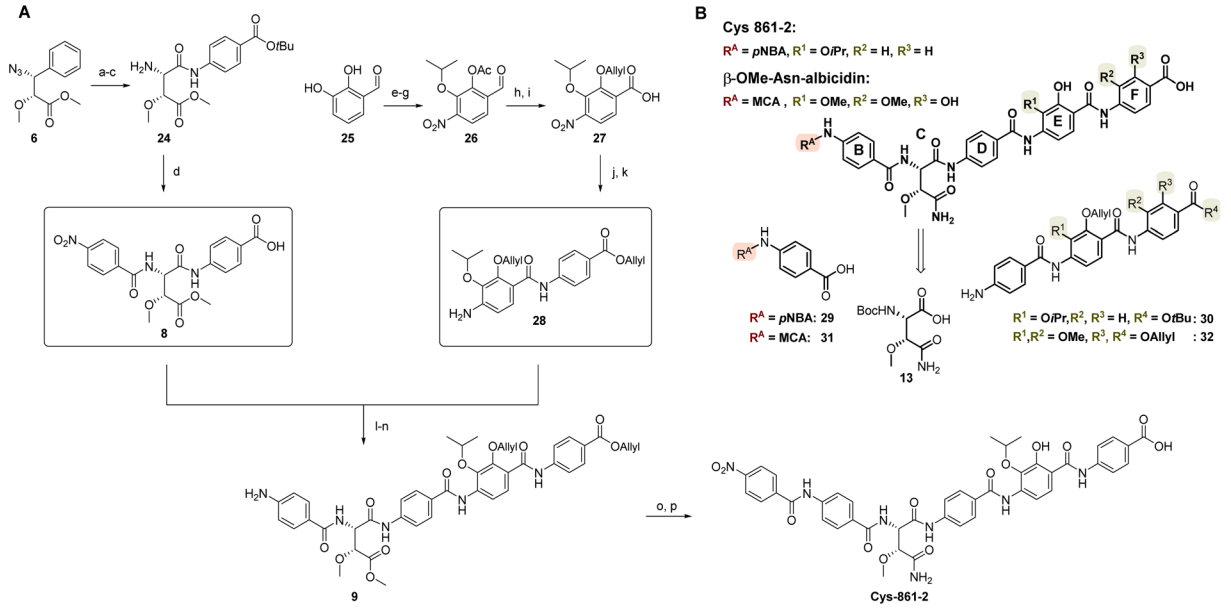


Fig. 14 (A) Total synthesis of **Cys 861-2**. Reagents and yields: (a) $RuCl_3$, $NaIO_4$, 71%; (b) $POCl_3$, *tert*-butyl 4-aminobenzoate, DIPEA, 81%; (c) $PPh_3$, $H_2O$; (d) 4-nitrobenzoyl chloride, 71% for 2 steps; (e) NaH, 2-bromopropane, 37%; (f) AcCl, pyridine, 74%; (g) conc. $HNO_3$, 97%; (h) (1) aq. LiOH, (2) allyl bromide, $K_2CO_3$, 81% for 2 steps; (i) $NaClO_2$, $NaH_2PO_4$, 2-methyl-2-butene, *t*BuOH, quant.; (j) DIPEA, $POCl_3$, 88%; (k) $SnCl_2 \cdot 2H_2O$, 83%; (l) $POCl_3$, DIPEA, 61%; (m) EtOH, Acetic acid, Zn dust; (n) $NH_3$ (7 N), 51% for 2 steps; (o) 4-nitrobenzoyl chloride, DIPEA; (p) $Pd(PPh_3)_4$, phenylsilane, 59% for 2 steps. (B) Retrosynthesis for the recent scalable assembly of **Cys 861-2** and β-OMe-Asn-albicidin. **29**, **13** and **30** were obtained in 80% (for 2 steps), 32% (for 9 steps) and 8% (for 10 steps), respectively.

cystobactamid 920-1 and its epimer 920-2, both linked by a β-amino acid, was also established, providing important insights on conformational implications.[108]

## 6 Structure–activity relationships

The successful total synthesis of albicidin and cystobactamids paved the way for subsequent structure activity relationship (SAR) studies, which aimed for an understanding of the pharmacophore of these natural products, followed by the identification of improved derivatives with a broadened antibacterial profile, improved resistance profile, increased solubility and increased chemical stability. The overall architecture of oligoarylamide antibiotics comprising all six fragments is imperative for biological activity. Deletion of any number of fragments results in complete loss of bioactivity[24,85,109,110] with the exception of moderately active cystobactamid 507 consisting of the fragments DEF.[15] Extension of the molecule at the C- or N-terminus by further pABA units also leads to inactive molecules.[24,36] Moreover, antibiotic activities have often determined using pathogen panels that differed on the species and/or the strain level. Therefore, SAR findings for albicidins and cystobactamids are discussed in tandem along the different fragments of the respective lead structure.

### 6.1 Fragment A

Albicidins fragment A is represented by methyl coumaric acid (MCA), which is known to intercalate into DNA during the catalytic cycle of the gyrase. Initial studies utilized the fragment **BCDEF**, which was an intermediate in the total synthesis, as synthetic platform for structural variations of the fragment A.[110]

Deletion of the hydroxy or methyl group of the MCA was acceptable, as coumaric or cinnamic acid derivatives were only slightly less active (Fig. 15A). Moving the hydroxy group to another position other than *para* resulted in diminished activity.[110] Replacement of the hydroxy-group improved (cyano-, fluoro-), retained (trifluoromethyl-, methoxy-, nitro-, ethynyl-), reduced (amino-, triazolyl-, carboxy-), or eliminated (tetrazolyl-) antibacterial activity.[105,110] Aromaticity of the N-terminal ring is not crucial, as a cyclohexane derivative had only slightly decreased activity.[110] Replacement of the MCA with a range of benzoic acids slightly decreased activity unless an activity-boosting substituent was located in the *para*-position.[111] Heterocycles like thiophene, thiazole, pyrazine and pyridazine retained the anti-Gram-negative activity, while furan and pyrrole had disappointingly low activities.[111] Removal of the MCA or replacement by simple aliphatic acids led to complete loss of activity.[110]

Replacement of the MCA by heterocycles like quinolines, quinolones or benzazoles led to derivatives with good to excellent activities.[107] This is particularly interesting because it demonstrates a certain promiscuity of the DNA-intercalating fragment A.[109] In addition to their convincing antibacterial activities, derivatives with improved physicochemical properties were identified. A methylquinoline derivative had a broad spectrum of activity, was considerably more hydrophilic and, unlike MCA containing derivatives, was not prone to photoisomerization.

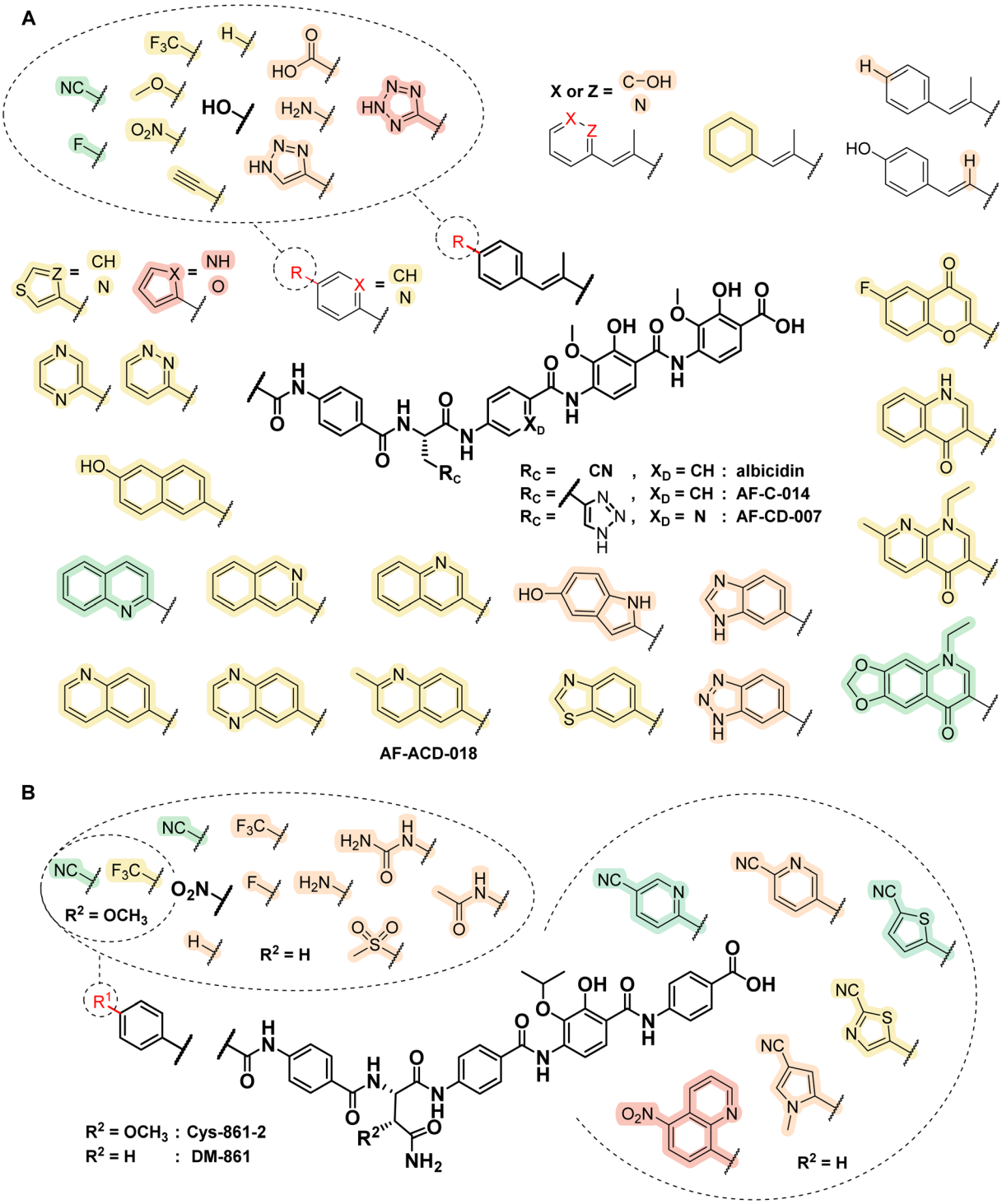


Fig. 15 Structure–activity relationship of fragment A for albicidins (A) and cystobactamids (B). Structural variations are highlighted and color-coded depending on their impact on the antibacterial activity. As references (bold structures), albicidin, **AF-C-014** or **AF-CD-007**, and cystobactamids **Cys 861-2** ($R^1 = NO_2$, $R^2 = OCH_3$) or DM-861 ($R^1 = NO_2$, $R^2 = H$) were used. Green = improved activity, yellow = retained activity, orange = reduced activity and red = no activity. Bold structures correspond to the lead structure.

Cystobactamids possess a benzoic acid fragment A. Since the naturally occurring cystobactamids like **Cys 861-2** [23] feature a *para*-nitro substituent, initial studies focused on the replacement of this potentially toxic group.[112] Simple substitution with a proton resulted in reduced antibacterial efficacy (Fig. 15B).[24] However, a cyano group was identified as a bioisostere with comparable electron-withdrawing and HBA properties, which enhanced broad-spectrum antibacterial activity. Other tested electron-withdrawing groups, such as trifluoromethyl, urea, methylsulfonyl, acetamide, and a fluorine atom, as well as the

 

electron-donating amino-group, exhibited reduced activity. Substitutions with $NO_2$- or $NH_2$-groups in the *ortho*- or *meta*-position were also poorly tolerated with respect to antibacterial activity (data not shown in Fig. 15).[24]

Heteroaromatic replacements of the phenyl ring were successfully achieved for DM-861 with a 5-cyano-substituted picolinamide and thiophene, as well as a 2-cyano-substituted thiazole. In contrast, derivatives such as nicotinic amide, pyrrole, and quinoline led to diminished activity against *P. aeruginosa* and *S. aureus*.[24]

### 6.2 Fragment B

Structural variations of the fragment B are rather underexplored, as no systematic study has been dedicated to this building block. The replacement of *p*ABA with 6-amino nicotinic acid, 5-amino picolinic acid or 6-amino pyridazine-3-carboxylic acid resulted in retention of activity of the related derivatives against Gram-negative bacteria although somewhat lower activity against Gram-positives (Fig. 17A).[78,113] Interestingly, a picolinamide showed improved gyrase activity, which can be rationalized by a possible hydrogen bond of the ring nitrogen to a phosphoester moiety in the inhibition complex of the gyrase bound DNA.[109]

### 6.3 Fragment C

The central amino acid of albicidin constitutes the hinge region of the molecule, as the α-amino acid links the two rigid aromatic arms. Alongside the total synthesis of the natural product, albicidin's enantiomer was characterized as well (Fig. 16A). The gyrase inhibition was not influenced by the chirality of Cya, although the antibacterial activity was significantly lower. A systematic study of fragment C identified L-Thr, dimethylamino-L-alanine, L-His, or 1-methyl-L-His as viable replacements of L-Cya.[114,115] The corresponding derivatives had comparable activities, were more hydrophilic and, unlike Cya, not prone to hydrolysis. The amino-isobutyric acid and the glycine derivative were slightly less active than the natural product against Gram-negatives, while the Gly derivative was disappointing against Gram-positive strains.[115] Charged amino acids such as Lys or Asp were not accepted in fragment C, as corresponding derivatives were inactive.[115] Since all these derivatives had potent gyrase activity,[115] the lower antibacterial activity might be explained by reduced accumulation in the bacterial cell. Introduction of highly hydrophilic amino acids like morpholino alanine or the three possible isomers of pyridyl alanine led to a slightly reduced activity, while incorporation of amino acids with a backbone cyclization like 4-amino-1-methylpiperidine-4-carboxylic acid or hydroxy-proline were inactive.[74,114] For potent bioactivity, a certain degree of flexibility of the hinge region might be required, which was impaired in the conformationally restrained C-variations. Ultimately, L-azahistidine (azaHis) was identified as superior replacement, resulting in improved antibacterial activities, increased water solubility and higher chemical stability.[13] The convincing properties of this modification can be explained by an additional hydrogen bond of the triazole with the water shell of the complexed magnesium$^{2+}$ ion in the catalytic pocket of gyrase, which led to an improved target affinity.[109] In general, L-amino acids tended to have slightly better MIC values than their D-enantiomers, which was demonstrated for Cya, dimethylamino alanine, His and azaHis derivatives.[94,114]

The natural cystobactamids 919-2 and 919-1 connect the AB rings to the eastern DEF half either by a (2*S*,3*R*)-β-methoxy-L-asparagine (β-MeO-L-Asn) moiety as in **Cys 919-2**, or by iso-(2*S*,3*R*)-α-methoxy-L-asparagine (α-MeO-L-isoAsn) as in **Cys 919-1**, but are otherwise identical.[16] Because 919-1 with the β-MeO-L-Asn had much higher antibiotic potency, all subsequently synthesized analogs were α-amino acids. With over 30 synthetic linker variations, the contribution of this central α-amino acid to the antibacterial activity of cystobactamids is well understood. An initial study by Testolin *et al.* demonstrated that the β-methoxy group in the fragment C side chain of **Cys 861-2**, which is synthetically demanding, was not essential for activity against *E. coli* and *S. aureus*.[24] The reduced activity against *P. aeruginosa* of DM-861 (Fig. 16B , DM: desmethoxy) with a simple L-Asn as fragment C was compensated by introducing 4-cyanobenzoic acid in fragment A, identifying the resulting derivative **CN-DM-861** (Fig. 16B) as a promising lead structure for further studies.

Subsequent research revealed that neither the hydrogen bond acceptor (HBA) nor the hydrogen bond donor (HBD) properties of the primary amide in **CN-DM-861** were essential for activity. Compounds with propargyl, vinyl, or amino groups attached to the β-position proved particularly active.[102] However, elongation of the side chain by one methylene group led to a reduction in antibacterial activity for both the alkyne and amine. Incorporation of a vinyl-substituted cyclopropane containing amino acid, with the α-carbon embedded in the ring, yielded a derivative with activity comparable to **CN-DM-861**. Other preferred groups at the β-position included a nitro group in racemic nitro-valine, which showed pronounced activity against *A. baumannii*, a hydroxy group as in L-allo-threonine, a triazole, and a cyclopropane ring. Methylation of either the β-amino or β-hydroxy groups negatively impacted antibacterial activity. Additionally, incorporating the backbone α-carbon and amine into a piperidine ring, thereby rigidifying the structure, led to a decline in broad-spectrum antibacterial activity, a phenomenon similar to that observed for albicidins with L-Hyp in fragment C. Despite having a diminished spectrum, such rigidifications were shown to lead to a stronger inhibition of *E. coli* gyrase and TI IV.[102] As demonstrated by three matched molecular pairs, α-L-amino acids were preferred over α-D-amino acids, as is the case with the albicidins (Fig. 16B). The replacement of the central α-amino acid with an unsubstituted *p*ABA (not shown in Fig. 16B) resulted in entirely linear compounds devoid of antibacterial activity.[36]

### 6.4 Fragment D

In a similar way to that described for fragment B, the *p*ABA moiety of fragment D in albicidin was replaced with 6-amino nicotinic acid and 5-amino picolinic acid (Fig. 17A). This pyridine scan revealed a picolinic acid derivative as superior with improved MIC values against Gram-positive bacteria. This

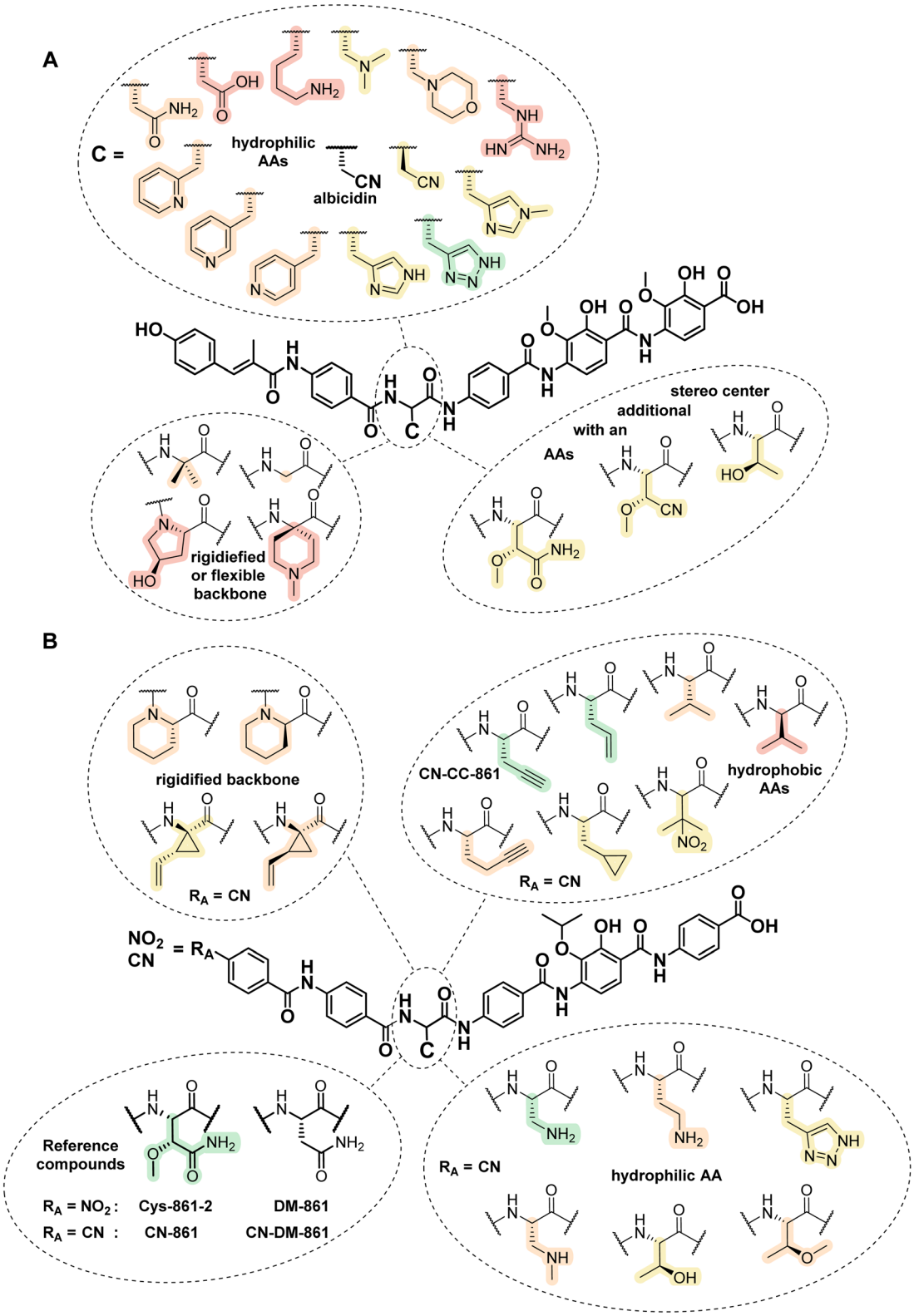


Fig. 16 Structure–activity relationship of the fragment C for albicidins (A) and cystobactamids (B). Structural variations are highlighted and color-coded depending on their impact on the antibacterial activity. As references (bold structures), albicidin and **CN-DM-861** were used. Green = improved activity, yellow = retained activity, orange = reduced activity and red = no activity. Bold structures correspond to the lead structure.

coincided with improved gyrase activity, which was explained by a pronounced effect of an intramolecular hydrogen bond (IMHB) of the ring nitrogen with the adjacent amide proton. Density functional theory (DFT) calculations showed that the IMHB led to a favorable planarization of the C-terminal arm of albicidin.[78] This could result in a better fit of the DEF fragment

 

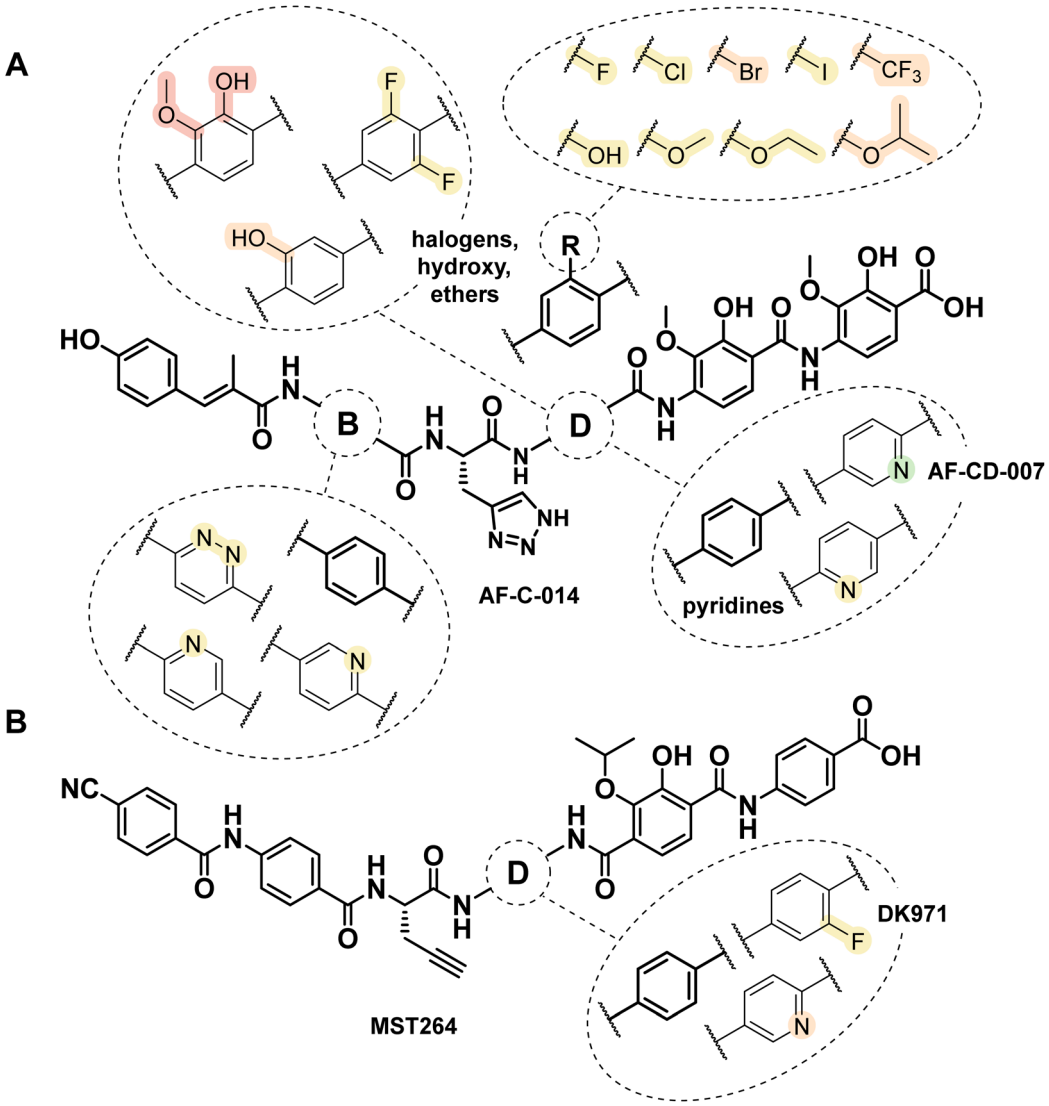


Fig. 17 Structure–activity relationship of fragments B and D for albicidins (A) and fragment D for cystobactamids (B). Structural variations are highlighted and color-coded depending on their impact on the antibacterial activity. As references (bold structures), **AF-C-014** and **MST264** were used. Green = improved activity, yellow = retained activity, orange = reduced activity and red = no activity. Bold structures correspond to the lead structure.

filling the space between the two opposing α3/α3′ helices in the subunit GyrA.[109] A nicotinic acid derivative, which does not feature the described planarization effect, had rather disappointing activities.[78] A panel of *p*ABA derivatives with substituents in the 2-position, were synthesized to exploit the effect of IMHB with the amide proton at the DE-link. Hydroxy-, fluoro- and chloro-variants were convincing as well, whereas trifluoromethyl-, bromo- and iodo-derivatives had reduced activities, especially against Gram-positive bacteria.[114,116] Moving the hydroxy-group to the 3-position of *p*ABA reduced the activity, and adding a methoxy-group to the 3-position led to a loss of activity.[114]

The structural variations of fragment D in cystobactamids remain relatively underexplored. While the introduction of a pyridine nitrogen atom in the case of the picolinic acid derivative resulted in reduced activity against *Klebsiella pneumoniae*, *Pseudomonas aeruginosa*, and *Streptococcus pneumoniae*, the incorporation of a 2-fluorine substituent maintained a high level of broad-spectrum activity (Fig. 17B).[117] The inverted DE amide in these cystobactamid derivatives may account for the contrasting results observed for picolinic acid containing derivatives of both classes, as it prevents the formation of a comparable IMHB between the ring nitrogen and the adjacent amide bond, which is present in the albicidin counterparts.

### 6.5 Fragment EF

The C-terminal fragment EF of albicidin is constituted by two 4-amino-2-hydroxy-3-methoxybenzoic acids. The substituents of these *p*ABA related building blocks are forming an IMHB network which is important for the bioactivity of the compound.[78] The role of each of these substituents was systematically evaluated by sequential deletions (Fig. 18A).[13] In general, removal of any number of substituents led to reduced

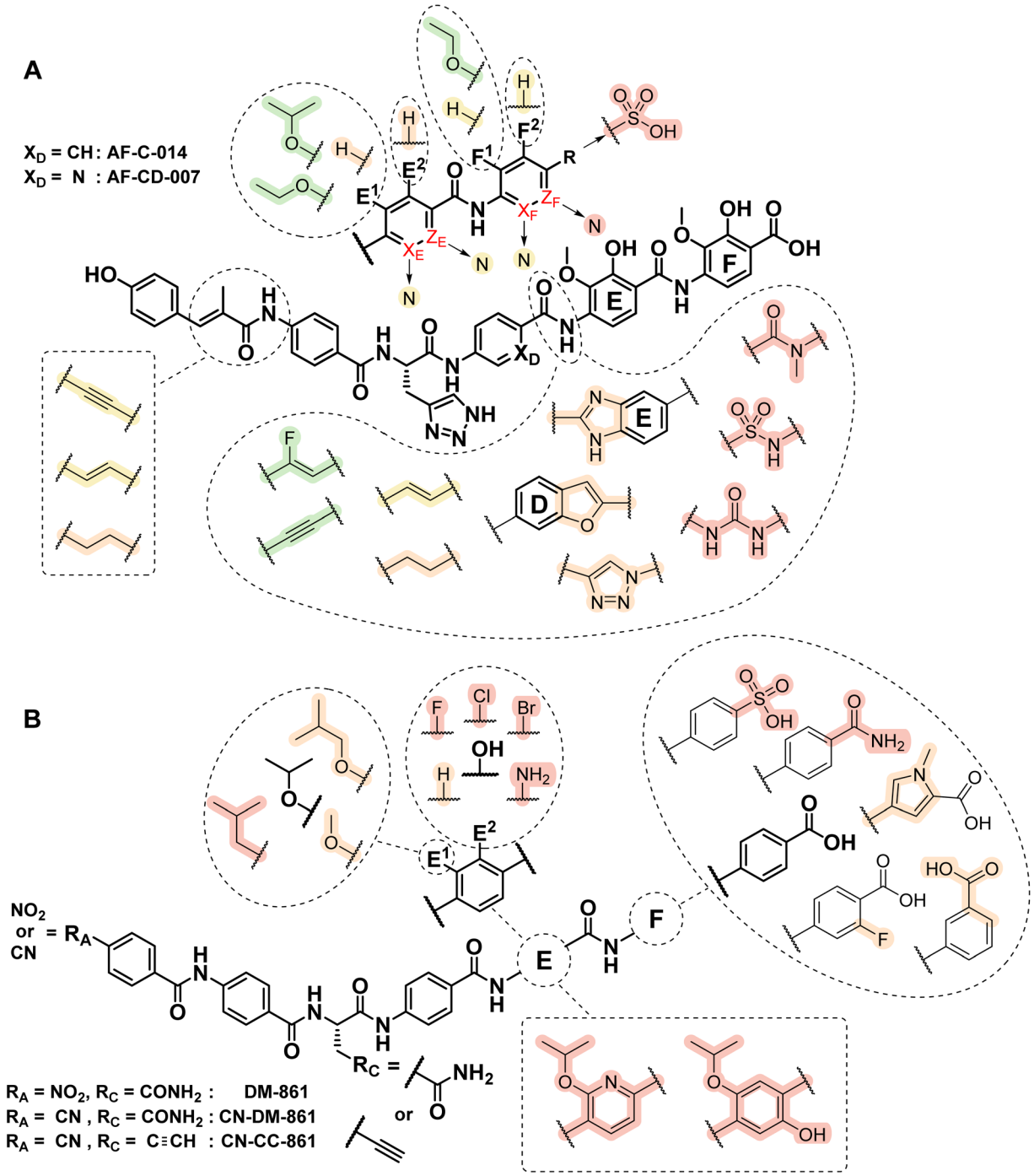


Fig. 18 Structure–activity relationship of fragments E and F, and amide bond isosteres for albicidins (A) and of fragments E and F for cystobactamids (B). Structural variations are highlighted and color-coded depending on their impact on the antibacterial activity. As references (bold structures), **AF-C-014** or **AF-CD-007** and cystobactamids DM-861861 ($R_A$ = $NO_2$, $R_C$ = $CONH_2$), **CN-DM-861** ($R_A$ = CN, $R_C$ = $CONH_2$) or **CN-CC-861** ($R_A$ = CN, $R_C$ = C≡CH) were used. Green = improved activity, yellow = retained activity, orange = reduced activity and red = no activity. Bold structures correspond to the lead structure.

activity, whereby deletions in fragment E exerted a more pronounced impact on the bioactivity in comparison to those in fragment F. In particular, the methoxy group in fragment E appears to be important for activity.[13] Besides its critical role in contributing to the IMHB network, it additionally occupies a hydrophobic pocket on the α3/α3′ helices in the GyrA subunit of the target gyrase.[109] Increasing the hydrophobicity of the alkoxy ethers by replacing methoxy groups with ethoxy or isopropoxy groups improved the antibacterial activity of the respective derivatives.[13] While nicotinic acids were accepted in fragment E and F, picolinic acid derivatives were only active in fragment E.[13,78] Picolinic acids in fragment F form an IMHB with

 

the carboxylic acid at the C-terminus, which appeared to be detrimental for the activity.[78] The carboxylic acid in fragment F is particularly critical, as deletion or replacement with sulfonic acids led to inactive derivatives.[13]

In cystobactamids, the phenolic OH was identified as an essential pharmacophore element, as its deletion[24] or substitution with a halogen atom (F, Cl, Br)[103] compromised broad-spectrum activity (Fig. 18B). Even the substitution with an amine, despite its hydrogen bond donor (HBD) properties, led to a significant loss of activity. Similarly, a pyridine derivative, which only possesses an HBA, was not a suitable substitute. Replacing the isopropoxy group by an isobutyl group, thereby removing an HBA, also diminished activity. Shifting the isopropyl group to the *para*-position relative to the phenol also rendered the compound inactive. For all the substitution patterns of fragment E described so far, the modified IMHB network presumably plays a decisive role.[103] Furthermore, increasing the size of the isopropoxy group to an isobutoxy group,[24] or reducing it to a methyl group,[103] as seen in the substitution pattern of albicidins, impaired activity, with potency limited to certain strains.

Substitution of the carboxylic acid in the F-fragment with a primary amide or the more acidic sulfonic acid resulted in a pronounced loss of activity, a similar effect as seen with the albicidins (Fig. 18B).[24] Shifting the carboxylic acid from the *para*- to the *meta*-position, as well as the integration of an *N*-methylpyrrole ring, both of which led to an altered conformation, significantly reduced activity. In contrast, the introduction of an additional *ortho*-fluorine atom caused only a slight decline in potency, except in the case of *P. aeruginosa*. Through C-terminal elongation with three additional *p*ABA units, the antibacterial activity also significantly decreased or disappeared entirely (not shown in Fig. 18B).[36]

### 6.6 Amide bond isosteres

Albicidins and cystobactamids consist of six building blocks that are connected by five amide bonds. As amide bonds can be hydrolyzed chemically or enzymatically, replacement by isosteric groups is a valid strategy to improve the stability of the lead structure. Amide isosteres were used to systematically replace amides along the oligoamide backbone: the acrylamide unit has been replaced by an ethynyl and (*E*)-vinyl link resulting in slightly shortened derivatives with increased activities (Fig. 18A). While the alkene very closely resembles the structure of an amide bond, the substitution with an alkyne leads to a shift in the relative positioning of fragments A and B. Nevertheless, both isosteres retain a stiff rod-shaped structure which was beneficial for the antibacterial activity. On the other hand, flexible linkers as ethyl or aminomethyl were also acceptable, as related derivatives retained their antibacterial properties.[105,116]

The DE amide is the crucial cleavage site for the resistance factor AlbD.[85] To prevent hydrolysis catalyzed by this protease, amide bond isosteres have been extensively studied in this position. Unfortunately, sulfonamides, *N*-methyl amides and urea substitutions led to inactive compounds. Replacement of the amide with heterocycles, *i.e.* a triazole, a fused benzofuran or a fused benzimidazole were better accepted, due to a less

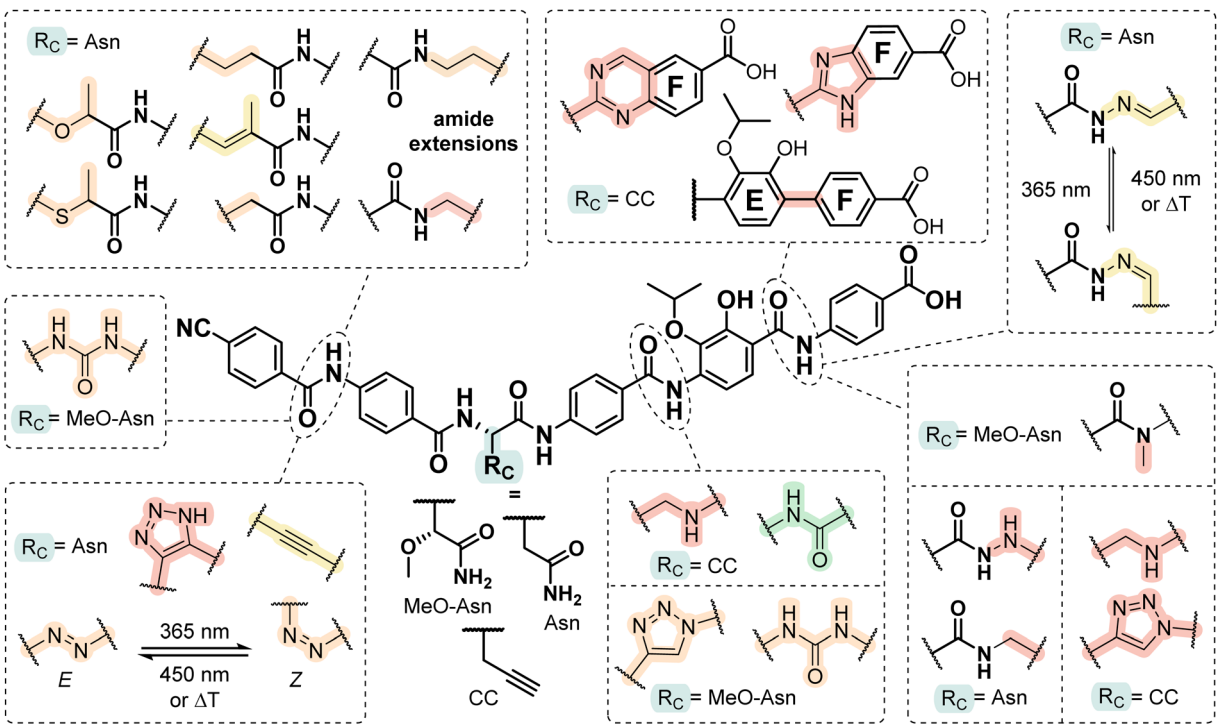


Fig. 19 Cystobactamid SAR of amide bioisosteres between fragments A/B, D/E and E/F. Structural variations are highlighted and color-coded depending on their impact on the antibacterial activity compared to **CN-DM-861** ($R_C$ = CH2C(O)NH2), **Cys 861-2** (A-fragment: *para*-NO2, $R_C$ = CH(OCH3)C(O)NH2) and **CN-CC-861** ($R_C$ = CH2C≡CH). Green = improved activity, orange = reduced activity and red = no activity.

pronounced conformational impact. Isosteres like (*E*)-vinyl, (*Z*)-fluorovinyl or ethynyl, that retain the rod-shaped structure of the C-terminal arm, had good to excellent antibacterial activities. The flexible ethyl link has a similar length as an amide bond but is lacking preorientation, which might be the reason for slightly reduced activity.

Due to its synthetic accessibility, the amide connecting the A and B fragments of cystobactamids has been extensively investigated. Structural modifications extending the length of the amide to an acrylamide linker, as seen in the MCA-1 of albicidins, have been shown to retain biological activity, particularly in analogues featuring a *para*-cyano-substituted methyl cinnamic acid (Fig. 19).[24] Other amide extensions by methylene, ethylene or (thio)ether group insertions,[24] replacement by an urea group or triazole ring,[104] resulted in reduced or abolished activity,[24] likely due to impaired spatial orientation of fragment A.[24]

The synthesis of photosensitive azobactamides aimed at developing an antimicrobial agent, whose activity can be controlled by light (Fig. 19). This approach offers potential advantages, such as local activation at the site of infection, thereby sparing commensal bacteria like the microbiome. The observed differences in antibiotic activity between (*E*)- and (*Z*)-isomers were insufficient to support practical applications in terms of an on–off switch. However, both isomers had different sensitivities towards the resistance factors AlbA and AlbD. The study represents the first example demonstrating how the sensitivity of an antibiotic towards resistance can be modulated by light.[118]

Analogous to the albicidins, the introduction of a urea or triazole moiety between fragments D and E resulted in reduced broad-spectrum activity.[24] However, in the case of the triazole, this modification effectively inhibited *in vitro* hydrolysis by the endopeptidase AlbD, whereas the corresponding amide **CN-DM-861** underwent almost complete cleavage following six hours of incubation.[24,104] Notably, inversion of the amide to a terephthalic acid derivative also conferred resistance to proteolytic degradation by AlbD while simultaneously enhancing broad-spectrum activity relative to **CN-CC-861**.[103] In contrast, the incorporation of a benzylamine moiety, which increased conformational flexibility, led to a complete loss of activity.[103]

For the amide between the fragments E and F, modifications such as an extension in the form of a hydrazide or an additional methylene group,[24] an altered angle between fragments E and F induced by a triazole, or increased rotational flexibility in benzylamine or biphenyl derivatives were not tolerated (Fig. 19).[103] Amide methylation, as well as the incorporation of benzimidazole or quinazoline as heterocycles, also resulted in a loss of activity.[103]

In summary, more than 700 derivatives of albicidins and cystobactamids were prepared by total synthesis. This number probably exceeds that of most natural product optimization programs, and it demonstrates the power of synthetic chemistry. The medicinal chemistry programs allowed the preparation of analogs with strongly increased antibiotic potency and improved drug properties. The best analogs were optimized at

Table 1 MIC values of selected oligoarylamide antibiotics

| | Compound | Albicidin | **AF-C-014** | | **AF-CD-007** | | **Cys 919-2** | | **Cys 919-1** | Coralmycin A | **CN-CC 861** | **DK971** | **CIP** [a] |
|---|---|---|---|---|---|---|---|---|---|---|---|---|---|
| Strains | Ref. | 78 | 78 | | 78 | | 15 and 23 | | 15 | 19 | 103 | 117 | 78 and 103 |
| *E. coli* | | 0.125[b] | 0.031[b] | | ≤0.016[b] | | 0.5[c] | 2[b] | 15–29[c] | 0.125[b,c] | ≤0.06[d] | ≤0.2[e] | ≤0.03[d,e] | 0.016[c] | 32[b] |
| *K. pneumoniae* | | 128[c] | 16[c] | 128[b] | 8[c] | 64[b] | >64[c] | | n.d. | 2[c] | 0.06–0.25[f] | | ≤0.03[f] | 0.063[c] | 128[b] |
| *A. baumannii* | | 2[b] | 2[b] | | ≤0.016[b] | | 8[c] | | >50[c] | 0.125[c] | 0.5–1[g] | | ≤0.03[g] | <0.25[k] | 32[b] |
| *P. aeruginosa* | | 2[b] | 8[b] | | 2[b] | | 64[c] | | n.d. | 4[c] | 0.5–16[h] | | 1[i] | 0.063[c] | 32[b] |
| *S. aureus* | | 4[b] | 0.5[b] | | 0.063[b] | | 0.1[c] | | 33[c] | 0.015[c] | 0.02[j] | | ≤0.03[j] | 0.125[c] | 128[b] |

[a] CIP = ciprofloxacin. [b] CIP resistant clinical isolate. [c] CIP susceptible clinical isolate. [d] Strain ATCC-25922 (WT). [e] Strain LM705 (S83L, D87N, S80I, Δ*acrR*, Δ*marR*; CIP resistant). [f] Strain KP10581 (CIP resistant). [g] Strain CIP-107292 (CIP resistant). [h] Strain Pa14 (WT). [i] Strain PAO1 (WT). [j] Strain ATCC-29213 (WT). [k] Strain DSM-30008.

2–4 positions compared to the natural products (Table 1). However, the overall molecular architecture of a hexapeptide with two conformationally restricted halves with aromatic character, linked by an α-amino acid that functions as a hinge, was retained in all highly active analogs.

## 7 *In vivo* studies

Up to date, three publications on *in vivo* experiments on albicidin or cystobactamid analogs (Fig. 20) have been reported. Following a single intravenous (i.v.) injection, a half-life of 1.2–1.4 hours was determined for **AF-C-014** and **AF-CD-007** in mice, similar to that for **CN-DM-861** with 1 h found at a 10-fold lower dose (Table 2).[24] The distribution volumes of all three substances were also similar with 2.7–4.9 L $kg^{-1}$. Subcutaneous injection (s.c.) of 5 mg $kg^{-1}$ **CN-DM-861** resulted in a slower accumulation and elimination, prolonged half-life of 1.7 h and a larger volume of distribution.

In a tolerability study in male CD-1 mice, two administrations of **AF-C-014** at 50 mg $kg^{-1}$, given 12 hours apart, did not induce side effects, macroscopic necropsy of internal organs or altered blood cell counts.[78] The *in vivo* activity of **AF-CD-007** was tested in a septicemia model against a fluoroquinolone-resistant *E. coli* clinical isolate.[78] The compound was administered in two doses of 6 or 17 mg $kg^{-1}$ two and 12 hours post infection (p.i.) (Table 3). A significant reduction in colony forming units (cfu) per g organ by 2.0 and 3.4 $log_{10}$ units was observed in the kidneys and the spleen at the higher dose, respectively (Fig. 21A).

**CN-DM-861** was tested in a neutropenic thigh infection model with *E. coli* (strain ATCC 25922).[24] The first dose was administered i.v. 2 h after infection in the efficacy study for rapid plasma accumulation, followed by three further s.c. injections, resulting in a total dose of 37.5 and 67.5 mg per kg per day, respectively. A reduction in the bacterial load in the muscle (5.1–5.2 $log_{10}$ units) and lung tissue (3.5–3.6 $log_{10}$ units) was observed 24 h p.i. for both dosing groups compared with the vehicle (Fig. 21B). Complete sterility was observed in the kidneys.

As no dose-dependent effect was observed, a further study was conducted with an optimized formulation allowing for i.v. administration 1, 7, 13 and 19 h p.i. (Dosing groups: 20 mg per kg per day, 40 mg per kg per day and 50 mg per kg per day). In all three groups, a reduction in cfu per gram thigh tissue was achieved compared to untreated mice 1 hour p.i. (Fig. 21C). However, with a cfu reduction of 4.0 $log_{10}$ units, the lowest dose was less active than the two higher doses achieving reductions of 5.3 and 4.9 $log_{10}$ units, respectively.

After **CN-CC-861** successfully completed a tolerability study at a dosage of four times 20 mg $kg^{-1}$ at 6 hour intervals, its efficacy was also tested in a neutropenic thigh infection model with a comparable dosage regimen.[102] Despite a similar MIC value against *E. coli* ATCC 25922 compared to **CN-DM-861**, the two lower doses (20 mg per kg per day and 40 mg per kg per day) were not efficacious, because a reduction in bacterial load of 2.2 $log_{10}$ units compared to the vehicle control was only observed at the highest dose of 80 mg per kg per day. The lower level of *in vivo* activity compared to **CN-DM-861** was attributed to the low solubility and high plasma protein binding of **CN-CC-861**. In general, increasing the solubility and reducing the plasma protein binding constitute important goals in the optimization programs of oligoarylamides. While the former is important to develop a parenteral formulation of the compounds, that are not orally bioavailable, the latter might further enhance the *in vivo* potency by increasing the fraction of unbound drug. However, introduction of solubilizing groups in the structure of oligoarylamides frequently led to an unfavorable activity profile, with a few exceptions, of respective compounds.

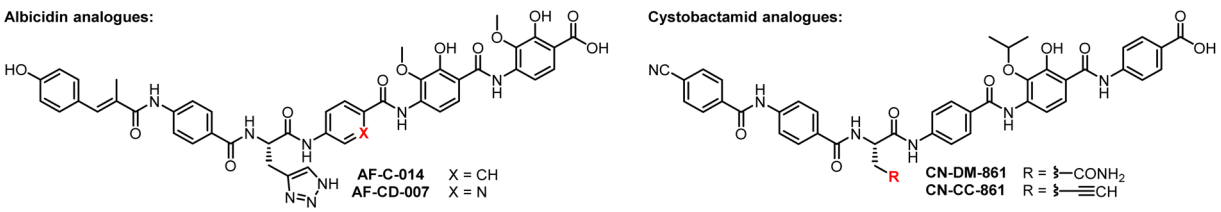


Fig. 20 Structures of albicidin and cystobactamid analogs evaluated *in vivo*.

Table 2 *In vivo* pharmacokinetic properties for AF-C-014, AF-CD-007 and CN-DM-861

| | **AF-C-014** | **AF-CD-007** | **CN-DM 861** | |
|---|---|---|---|---|
| Mice[a] | Male CD-1 | Male CD-1 | Male CD-1 | |
| Application route | i.v.[b] | i.v.[b] | i.v.[b] | s.c.[c] |
| Dose [mg $kg^{-1}$] | 50 | 50 | 5 | 5 |
| AUC [ng h $mL^{-1}$] | 153 320 ± 47 239 | 224 852 ± 49 029 | 2087 ± 573 | 517 ± 64 |
| Half-life $t_{1/2}$ [h] | 1.2 ± 0.6 | 1.4 ± 1.5 | 0.98 ± 0.1 | 1.65 ± 0.4 |
| Vz [L $kg^{-1}$] | 4.9 ± 5.2 | 2.7 ± 1.1 | 3.5 ± 1.2 | 22.8 ± 3.1 |

[a] Three mice were used in each experiment. [b] Intravenous application. [c] Subcutaneous administration.

Table 3 *In vivo* efficacy studies of **AF-CD-007**, **CN-DM-861** and **CN-CC-861** in male CD-1 mice

| Model | Pathogen | Compd | MIC [μg mL$^{-1}$] | Dosage |
|---|---|---|---|---|
| Septicemia | CIP-resistant *E. coli* clinical isolate number 191950584 | **AF-CD-007** | 0.031 | 2× daily dosing i.v.<br>Single dose: 6 or 17 mg kg$^{-1}$<br>$t$ = 2 and 12 h p.i. |
| Neutropenic thigh infection | *E. coli* ATCC 25922 | **CN-DM-861** | 0.02 | 4× daily dosing<br>Group 1: 7.5 mg kg$^{-1}$ i.v. ($t$ = 2 h p.i.), followed by 10 mg kg$^{-1}$ s.c. ($t$ = 4, 8 and 12 h p.i.)<br>Group 2: 7.5 mg kg$^{-1}$ i.v. ($t$ = 2 h p.i.), followed by 20 mg kg$^{-1}$ s.c. ($t$ = 4, 8 and 12 h p.i.)<br>4× daily dosing i.v.<br>Single dose: 5, 10 or 12.5 mg kg$^{-1}$<br>$t$ = 1, 7, 13 and 19 h p.i. |
| | | **CN-CC-861** | 0.03 | 4× daily dosing i.v.<br>Single dose: 5, 10 or 20 mg kg$^{-1}$<br>$t$ = 1, 7, 13 and 19 h p.i. |

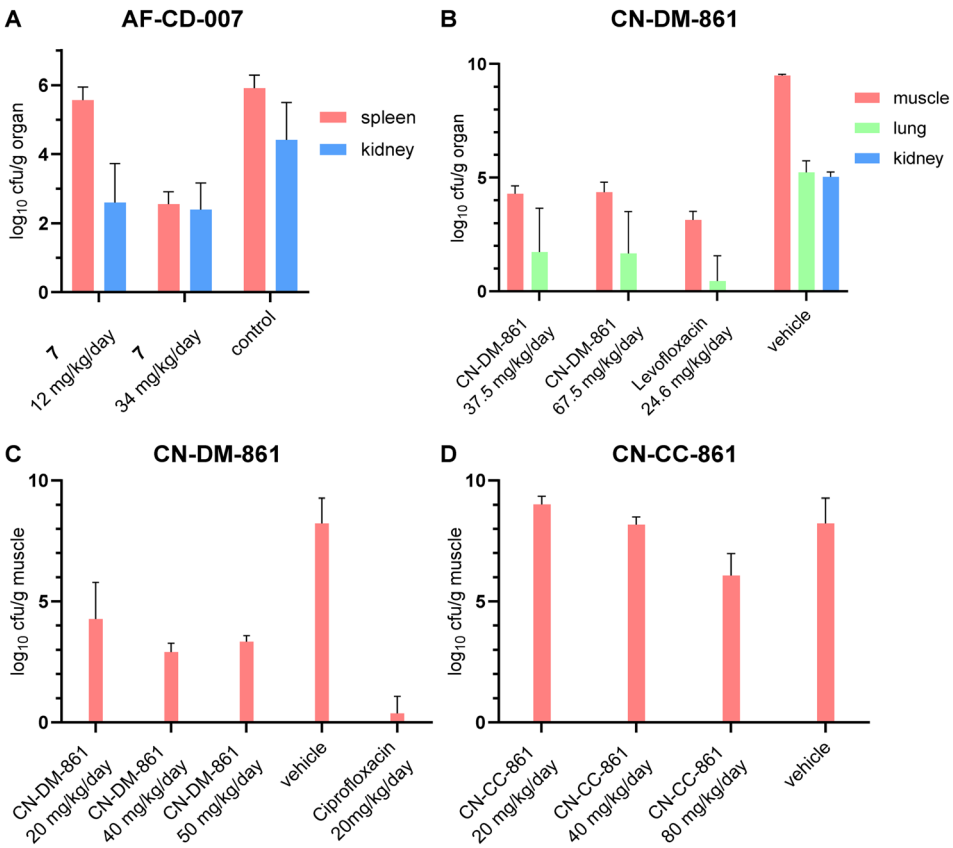


Fig. 21 Results of *in vivo* efficacy studies listed in Table 3.

In summary, both albicidin and cystobactamid derivatives have exhibited strong *in vivo* activity in rodent infection models and demonstrated high tolerability in mice, even at elevated doses.

## 8 Conclusions

The chemical structures of albicidin and cystobactamid have been first reported about a decade ago. Since then, their potential as antibiotics has been recognized and leveraged by more than 62 systematic studies covering biosynthesis, chemical synthesis, microbiology and pharmacology. This led to a profound understanding of their mode of action on molecular and cellular levels, their antibiotic and pharmacological properties, resistance mechanisms, and structure–activity relationships. For both series, the original natural products have been replaced by chemically synthesised analogs with superior drug properties. Nevertheless, key structural elements of the natural

 

products were preserved, underscoring their crucial role in mediating a unique binding mechanism. These elements are essential for locking the cleaved gyrase–DNA intermediates in place through interactions with both the DNA and the protein helices. Despite decades of research on gyrase inhibitors and a profound understanding of their target, no synthetic or computational approaches have led to compounds of interest with a similar mechanism or chemistry. The oligoarylamides are one of few examples for a new antibiotic series that breaks resistance and displays a broad spectrum that covers all Gram-positive and Gram-negative priority pathogens. This has been achieved through a medicinal chemistry program involving >700 analogs. This scope also demonstrates that medicinal chemistry programs based on natural product hits are technically feasible nowadays. The most promising analogs have shown *in vivo* efficacy across multiple infection models and have progressed to the end of the lead optimization phase. In summary, these results underscore the continued importance of exploring natural products as sources of novel antibiotics.

## 9 Conflicts of interest

MK-K, MB, DK, DH and RDS are coinventors on patent applications on natural and synthetic albicidins and cystobactamids.

## 10 Data availability

No primary research results, software or code have been included and no new data were generated or analysed as part of this review.

## 11 Acknowledgements

We thank Dr John Weston (Kelkheim, Germany) for critical reading of the manuscript. Financial support was granted by the Deutsche Forschungsgemeinschaft (DFG, RTG 2473 'Bioactive Peptides', project number 392923329) (PG, RDS), the State of Berlin (Elsa-Neumann-Stipendium für Promovierende, T70011) (MK-K), the BMBF for the project OpCyBac (16 GW0219K), and the German Center for Infection Research (TTU09.722).

## 12 References

1 M. Naghavi, S. E. Vollset, K. S. Ikuta and C. J. L. Murray, *Lancet*, 2024, **404**, 1199–1226.
2 R. D. Süssmuth, M. Kulike-Koczula, P. Gao and S. Kosol, *Angew. Chem., Int. Ed.*, 2025, **64**, e202414325.
3 D. Heimann, D. Kohnhäuser, A. J. Kohnhäuser and M. Brönstrup, *Drugs*, 2025, **85**, 293–323.
4 U. Theuretzbacher, K. Outterson, A. Engel and A. Karlén, *Nat. Rev. Microbiol.*, 2020, **18**, 275–285.
5 K. Lewis, *Cell*, 2020, **181**, 29–45.
6 K. Lewis, R. E. Lee, H. Brötz-Oesterhelt, S. Hiller, M. V. Rodnina, T. Schneider, M. Weingarth and I. Wohlgemuth, *Nature*, 2024, **632**, 39–49.
7 R. G. Birch and S. S. Patil, *J. Gen. Microbiol.*, 1985, **131**, 1069–1075.
8 R. G. Birch and S. S. Patil, *CA Pat.*, CA1228824A, 1987.
9 R. G. Birch and S. S. Patil, *Phytopathology*, 1983, **73**, 1368–1374.
10 M. J. Gasson, *Appl. Environ. Microbiol.*, 1980, **39**, 25–29.
11 R. M. Schwartz and M. O. Dayhoff, *Science*, 1978, **199**, 395–403.
12 S. M. Hashimi, M. K. Wall, A. B. Smith, A. Maxwell and R. G. Birch, *Antimicrob. Agents Chemother.*, 2007, **51**, 181–187.
13 I. Behroz, P. Durkin, S. Grätz, M. Seidel, L. Rostock, M. Spinczyk, J. B. Weston and R. D. Süssmuth, *Chem.–Eur. J.*, 2019, **25**, 16538–16543.
14 S. Cociancich, A. Pesic, D. Petras, S. Uhlmann, J. Kretz, V. Schubert, L. Vieweg, S. Duplan, M. Marguerettaz, J. Noëll, I. Pieretti, M. Hügelland, S. Kemper, A. Mainz, P. Rott, M. Royer and R. D. Süssmuth, *Nat. Chem. Biol.*, 2015, **11**, 195–197.
15 S. Baumann, J. Herrmann, R. Raju, H. Steinmetz, K. I. Mohr, S. Hüttel, K. Harmrolfs, M. Stadler and R. Müller, *Angew. Chem., Int. Ed.*, 2014, **53**, 14605–14609.
16 Y. Wang, B. Schnell, S. Baumann, R. Müller and T. P. Begley, *J. Am. Chem. Soc.*, 2017, **139**, 1742–1745.
17 W. A. M. Elgaher, M. M. Hamed, S. Baumann, J. Herrmann, L. Siebenbürger, J. Krull, K. Cirnski, A. Kirschning, M. Brönstrup, R. Müller and R. W. Hartmann, *Chem.–Eur. J.*, 2020, **26**, 7219–7225.
18 Y. Wang and T. P. Begley, *J. Am. Chem. Soc.*, 2020, **142**, 9944–9954.
19 Y. J. Kim, H.-J. Kim, G.-W. Kim, K. Cho, S. Takahashi, H. Koshino and W.-G. Kim, *J. Nat. Prod.*, 2016, **79**, 2223–2228.
20 R. Finking and M. A. Marahiel, *Annu. Rev. Microbiol.*, 2004, **58**, 453–488.
21 R. D. Süssmuth and A. Mainz, *Angew. Chem., Int. Ed.*, 2017, **56**, 3770–3821.
22 S. Groß, B. Schnell, P. A. Haack, D. Auerbach and R. Müller, *Nat. Commun.*, 2021, **12**, 1696.
23 S. Hüttel, G. Testolin, J. Herrmann, T. Planke, F. Gille, M. Moreno, M. Stadler, M. Brönstrup, A. Kirschning and R. Müller, *Angew. Chem., Int. Ed.*, 2017, **56**, 12760–12764.
24 G. Testolin, K. Cirnski, K. Rox, H. Prochnow, V. Fetz, C. Grandclaudon, T. Mollner, A. Baiyoumy, A. Ritter, C. Leitner, J. Krull, J. van den Heuvel, A. Vassort, S. Sordello, M. M. Hamed, W. A. M. Elgaher, J. Herrmann, R. W. Hartmann, R. Müller and M. Brönstrup, *Chem. Sci.*, 2020, **11**, 1316–1334.
25 D. Petras, D. Kerwat, A. Pesic, B.-F. Hempel, L. von Eckardstein, S. Semsary, J. Arasté, M. Marguerettaz, M. Royer, S. Cociancich and R. D. Süssmuth, *ACS Chem. Biol.*, 2016, **11**, 1198–1204.
26 L. von Eckardstein, D. Petras, T. Dang, S. Cociancich, S. Sabri, S. Grätz, D. Kerwat, M. Seidel, A. Pesic, P. C. Dorrestein, M. Royer, J. B. Weston and R. D. Süssmuth, *Chem. Weinh. Bergstr. Ger.*, 2017, **23**, 15316–15321.

27 Z. Wang, A. Kasper, R. Mehmood, M. Ternei, S. Li, J. S. Freundlich and S. F. Brady, *Angew. Chem.*, 2021, **133**, 22346–22351.
28 Z. Wang, N. Forelli, Y. Hernandez, M. Ternei and S. F. Brady, *Nat. Commun.*, 2022, **13**, 842.
29 Z. Wang, A. Kasper, M. Takahashi, A. Morales Amador, A. Bhattacharjee, J. Kan, Y. Hernandez, M. Ternei and S. F. Brady, *Angew. Chem., Int. Ed.*, 2024, **63**, e202317187.
30 E. Michalczyk, Z. Pakosz-Stępień, J. D. Liston, O. Gittins, M. Pabis, J. G. Heddle and D. Ghilarov, *Proc. Natl. Acad. Sci. U. S. A.*, 2024, **121**, e2407398121.
31 D. Sutormin, N. Rubanova, M. Logacheva, D. Ghilarov and K. Severinov, *Nucleic Acids Res.*, 2019, **47**, 1373–1388.
32 C. L. Baird, T. T. Harkins, S. K. Morris and J. E. Lindsley, *Proc. Natl. Acad. Sci. U. S. A.*, 1999, **96**, 13685–13690.
33 A. Gubaev and D. Klostermeier, *DNA Repair*, 2014, **16**, 23–34.
34 A. Gubaev and D. Klostermeier, *Proc. Natl. Acad. Sci. U. S. A.*, 2011, **108**, 14085–14090.
35 E. Michalczyk, K. Hommernick, I. Behroz, M. Kulike, Z. Pakosz-Stępień, L. Mazurek, M. Seidel, M. Kunert, K. Santos, H. Von Moeller, B. Loll, J. B. Weston, A. Mainz, J. G. Heddle, R. D. Süssmuth and D. Ghilarov, *Nat. Catal.*, 2023, **6**, 52–67.
36 D. Solga, L. H. E. Wieske, S. Wilcox, C. Zeilinger, L. Jansen-Olliges, K. Cirnski, J. Herrmann, R. Müller, M. Erdelyi and A. Kirschning, *Chem.–Eur. J.*, 2024, **30**, e202303796.
37 R. Franke, H. Overwin, S. Häussler and M. Brönstrup, *mSystems*, 2021, **6**, e00610–e00621.
38 P. Ashwath, P. Osiecki, D. Weiner, L. E. Via and J. P. Sarathy, *ACS Infect. Dis.*, 2024, **10**, 3631–3639.
39 P. D. Cotter, R. P. Ross and C. Hill, *Nat. Rev. Microbiol.*, 2013, **11**, 95–105.
40 L. Turnbull, M. Toyofuku, A. L. Hynen, M. Kurosawa, G. Pessi, N. K. Petty, S. R. Osvath, G. Cárcamo-Oyarce, E. S. Gloag, R. Shimoni, U. Omasits, S. Ito, X. Yap, L. G. Monahan, R. Cavaliere, C. H. Ahrens, I. G. Charles, N. Nomura, L. Eberl and C. B. Whitchurch, *Nat. Commun.*, 2016, **7**, 11220.
41 I. N. Wang, D. L. Smith and R. Young, *Annu. Rev. Microbiol.*, 2000, **54**, 799–825.
42 K. A. McFarland, E. L. Dolben, M. LeRoux, T. K. Kambara, K. M. Ramsey, R. L. Kirkpatrick, J. D. Mougous, D. A. Hogan and S. L. Dove, *Proc. Natl. Acad. Sci. U. S. A.*, 2015, **112**, 8433–8438.
43 M. F. Chellat, L. Raguž and R. Riedl, *Angew. Chem., Int. Ed.*, 2016, **55**, 6600–6626.
44 S. E. Rossiter, M. H. Fletcher and W. M. Wuest, *Chem. Rev.*, 2017, **117**, 12415–12474.
45 E. Peterson and P. Kaur, *Front. Microbiol.*, 2018, **9**, 2928.
46 S. Mak, Y. Xu and J. R. Nodwell, *Mol. Microbiol.*, 2014, **93**, 391–402.
47 J. M. Bostock, G. Huang, S. M. Hashimi, L. Zhang and R. G. Birch, *J. Appl. Microbiol.*, 2006, **101**, 151–160.
48 W. V. Basnayake and R. G. Birch, *Microbiol. Read. Engl.*, 1995, **141**, 551–560.
49 M. J. Walker, R. G. Birch and J. M. Pemberton, *Mol. Microbiol.*, 1988, **2**, 443–454.
50 M. Saathoff, S. Kosol, T. Semmler, K. Tedin, N. Dimos, J. Kupke, M. Seidel, F. Ghazisaeedi, M. C. Jonske, S. A. Wolf, B. Kuropka, W. Czyszczoń, D. Ghilarov, S. Grätz, J. G. Heddle, B. Loll, R. D. Süssmuth and M. Fulde, *PLoS Biol.*, 2023, **21**, e3002186.
51 L. Zhang and R. G. Birch, *Lett. Appl. Microbiol.*, 1996, **22**, 132–136.
52 R. G. Birch, J. M. Pemberton and W. V. S. Basnayake, *Microbiology*, 1990, **136**, 51–58.
53 T. S. Crofts, A. J. Gasparrini and G. Dantas, *Nat. Rev. Microbiol.*, 2017, **15**, 422–434.
54 Y.-Y. Huang, J.-Y. Deng, J. Gu, Z.-P. Zhang, A. Maxwell, L.-J. Bi, Y.-Y. Chen, Y.-F. Zhou, Z.-N. Yu and X.-E. Zhang, *Nucleic Acids Res.*, 2006, **34**, 5650–5659.
55 A. J. Ruthenburg, D. M. Graybosch, J. C. Huetsch and G. L. Verdine, *J. Biol. Chem.*, 2005, **280**, 26177–26184.
56 H. Yoshida, M. Bogaki, M. Nakamura and S. Nakamura, *Antimicrob. Agents Chemother.*, 1990, **34**, 1271–1272.
57 K. J. Aldred, R. J. Kerns and N. Osheroff, *Biochemistry*, 2014, **53**, 1565–1574.
58 S. M. Hashimi, G. Huang, A. Maxwell and R. G. Birch, *Antimicrob. Agents Chemother.*, 2008, **52**, 1382–1390.
59 J. Heddle and A. Maxwell, *Antimicrob. Agents Chemother.*, 2002, **46**, 1805–1815.
60 A. Confreres and A. Maxwell, *Mol. Microbiol.*, 1992, **6**, 1617–1624.
61 M. W. Vetting, S. S. Hegde, J. E. Fajardo, A. Fiser, S. L. Roderick, H. E. Takiff and J. S. Blanchard, *Biochemistry*, 2006, **45**, 1–10.
62 M. W. Vetting, S. S. Hegde, Y. Zhang and J. S. Blanchard, *Acta Crystallogr., Sect. F:Struct. Biol. Cryst. Commun.*, 2011, **67**, 296–302.
63 S. S. Hegde, M. W. Vetting, S. L. Roderick, L. A. Mitchenall, A. Maxwell, H. E. Takiff and J. S. Blanchard, *Science*, 2005, **308**, 1480–1483.
64 M. W. Vetting, S. S. Hegde, M. Wang, G. A. Jacoby, D. C. Hooper and J. S. Blanchard, *J. Biol. Chem.*, 2011, **286**, 25265–25273.
65 Ł. Mazurek, D. Ghilarov, E. Michalczyk, Z. Pakosz, M. Metelev, W. Czyszczoń, K. Wawro, I. Behroz, S. Dubiley, R. D. Süssmuth and J. G. Heddle, *Nucleic Acids Res.*, 2021, **49**, 1581–1596.
66 K. H. Almabruk, L. K. Dinh and B. Philmus, *ACS Chem. Biol.*, 2018, **13**, 1426–1437.
67 S. S. Pao, I. T. Paulsen and M. H. Saier, *Microbiol. Mol. Biol. Rev.*, 1998, **62**, 1–34.
68 E. Schmutz, A. Mühlenweg, S.-M. Li and L. Heide, *Antimicrob. Agents Chemother.*, 2003, **47**, 869–877.
69 M. A. Fernández-Moreno, J. L. Caballero, D. A. Hopwood and F. Malpartida, *Cell*, 1991, **66**, 769–780.
70 C. Fang, L. Li, Y. Zhao, X. Wu, S. J. Philips, L. You, M. Zhong, X. Shi, T. V. O'Halloran, Q. Li and Y. Zhang, *Nat. Commun.*, 2020, **11**, 6284.

 

71 C. Fang, S. J. Philips, X. Wu, K. Chen, J. Shi, L. Shen, J. Xu, Y. Feng, T. V. O'Halloran and Y. Zhang, *Nat. Chem. Biol.*, 2021, **17**, 57–64.
72 Y. Yang, C. Liu, W. Zhou, W. Shi, M. Chen, B. Zhang, D. G. Schatz, Y. Hu and B. Liu, *Nat. Commun.*, 2021, **12**, 2702.
73 C. Fang and Y. Zhang, *Acta Biochim. Biophys. Sin.*, 2022, **54**, 25–36.
74 S. Kosol, L. Rostock, J. Barsig, T. Tabarelli, K. Hommernick, M. Kulike, T. F. Eulberg, M. Seidel, I. Behroz, L. Kleebauer, S. Grätz, A. Mainz and R. D. Süssmuth, *Chem. Sci.*, 2023, **14**, 5069–5078.
75 C. Fang, L. Li, Y. Zhao, X. Wu, S. J. Philips, L. You, M. Zhong, X. Shi, T. V. O'Halloran, Q. Li and Y. Zhang, *Nat. Commun.*, 2020, **11**, 6284.
76 L. Rostock, R. Driller, S. Grätz, D. Kerwat, L. von Eckardstein, D. Petras, M. Kunert, C. Alings, F.-J. Schmitt, T. Friedrich, M. C. Wahl, B. Loll, A. Mainz and R. D. Süssmuth, *Nat. Commun.*, 2018, **9**, 3095.
77 A. Sikandar, K. Cirnski, G. Testolin, C. Volz, M. Brönstrup, O. V. Kalinina, R. Müller and J. Koehnke, *J. Am. Chem. Soc.*, 2018, **140**, 16641–16649.
78 L. Zborovsky, L. Kleebauer, M. Seidel, A. Kostenko, L. von Eckardstein, F. Otto Gombert, J. Weston and R. D. Süssmuth, *Chem. Sci.*, 2021, **12**, 14606–14617.
79 D. I. Andersson and D. Hughes, *Annu. Rev. Genet.*, 2009, **43**, 167–195.
80 L. Sandegren and D. I. Andersson, *Nat. Rev. Microbiol.*, 2009, **7**, 578–588.
81 M. Saathoff, K. Tedin, S. Grätz, P. Schwerk, M. Kunert, R. D. Süssmuth and M. Fulde, *J. Antimicrob. Chemother.*, 2023, **78**, 2102–2104.
82 T. Risch, D. Kolling, D. Mostert, T. Seedorf, D. Heimann, D. Kohnhäuser, F. Deschner, F. Fries, D. Solga, J.-S. Hilgers, J. Dastbaz, S. Mancini, A. K. H. Hirsch, M. Brönstrup, A. Kirschning, S. A. Sieber, J. Herrmann and R. Müller, *npj Antimicrob. Resist.*, 2024, **2**, 33.
83 L. Zhang and R. G. Birch, *Lett. Appl. Microbiol.*, 1996, **22**, 132–136.
84 L. Zhang and R. G. Birch, *Proc. Natl. Acad. Sci. U. S. A.*, 1997, **94**, 9984–9989.
85 L. Vieweg, J. Kretz, A. Pesic, D. Kerwat, S. Grätz, M. Royer, S. Cociancich, A. Mainz and R. D. Süssmuth, *J. Am. Chem. Soc.*, 2015, **137**, 7608–7611.
86 L. Zhang and R. G. Birch, *Proc. Natl. Acad. Sci. U.S.A.*, 1997, **94**, 9984–9989.
87 C. Maier, E. Bremer, A. Schmid and R. Benz, *J. Biol. Chem.*, 1988, **263**, 2493–2499.
88 A. Nieweg and E. Bremer, *Microbiol. Read. Engl.*, 1997, **143**, 603–615.
89 H. Fsihi, B. Kottwitz and E. Bremer, *J. Biol. Chem.*, 1993, **268**, 17495–17503.
90 R. G. Birch, J. M. Pemperton and W. V. S. Basnayake, *Microbiology*, 1990, **136**, 51–58.
91 E. Bremer, P. Gerlach and A. Middendorf, *J. Bacteriol.*, 1988, **170**, 108–116.
92 N. Amin and A. Peterkofsky, *J. Biol. Chem.*, 1995, **270**, 11803–11805.
93 P. Gerlach, L. Søgaard-Andersen, H. Pedersen, J. Martinussen, P. Valentin-Hansen and E. Bremer, *J. Bacteriol.*, 1991, **173**, 5419–5430.
94 J. Kretz, D. Kerwat, V. Schubert, S. Grätz, A. Pesic, S. Semsary, S. Cociancich, M. Royer and R. D. Süssmuth, *Angew Chem. Int. Ed. Engl.*, 2015, **54**, 1969–1973.
95 U. Wriede, M. Fernandez, K. F. West, D. Harcour and H. W. Moore, *J. Org. Chem.*, 1987, **52**, 4485–4489.
96 S. Kato and T. Morie, *J. Heterocycl. Chem.*, 1996, **33**, 1171–1178.
97 S. Hüttel, G. Testolin, J. Herrmann, T. Planke, F. Gille, M. Moreno, M. Stadler, M. Brönstrup, A. Kirschning and R. Müller, *Angew. Chem.*, 2017, **129**, 12934–12938.
98 B. Cheng, R. Müller and D. Trauner, *Angew. Chem.*, 2017, **129**, 12929–12933.
99 Z.-M. Wang, H. C. Kolb and K. B. Sharpless, *J. Org. Chem.*, 1994, **59**, 5104–5105.
100 A. Breuning, R. Vicik and T. Schirmeister, *Tetrahedron: Asymmetry*, 2003, **14**, 3301–3312.
101 M. Moeller, M. D. Norris, T. Planke, K. Cirnski, J. Herrmann, R. Müller and A. Kirschning, *Org. Lett.*, 2019, **21**, 8369–8372.
102 D. Kohnhäuser, T. Seedorf, K. Cirnski, D. Heimann, J. Coetzee, S. Sordello, J. Richter, M. Stappert, J.-F. Sabuco, D. Corbett, E. Bacqué, K. Rox, J. Herrmann, A. Vassort, R. Müller, A. Kirschning and M. Brönstrup, *J. Med. Chem.*, 2024, **67**, 17162–17190.
103 M. Stappert, D. Kohnhäuser, T. Seedorf, J. Coetzee, K. Rox, H. L. S. Fuchs, K. Cirnski, C. Leitner, J. Herrmann, A. Kirschning, R. Müller and M. Brönstrup, *Commun. Chem.*, 2024, **7**, 1–15.
104 T. Planke, K. Cirnski, J. Herrmann, R. Müller and A. Kirschning, *Chem.–Eur. J.*, 2020, **26**, 4289–4296.
105 I. Behroz, L. Kleebauer, K. Hommernick, M. Seidel, S. Grätz, A. Mainz, J. B. Weston and R. D. Süssmuth, *Chem.–Eur. J.*, 2021, **27**, 9077–9086.
106 L. Kleebauer, L. Zborovsky, K. Hommernick, M. Seidel, J. B. Weston and R. D. Süssmuth, *Org. Lett.*, 2021, **23**, 7023–7027.
107 M. Kulike-Koczula, K. Hommernick, L. B. Ghimire, S. Kosol, L. Zborovsky, M. Seidel, N. Sattler, A. Mainz, J. B. Weston, D. Ghilarov and R. D. Süssmuth, *Chem.–Eur. J.*, 2025, **31**, e202500162.
108 T. Planke, M. Moreno, S. Hüttel, J. Fohrer, F. Gille, M. D. Norris, M. Siebke, L. Wang, R. Müller and A. Kirschning, *Org. Lett.*, 2019, **21**, 1359–1363.
109 E. Michalczyk, K. Hommernick, I. Behroz, M. Kulike, Z. Pakosz-Stępień, L. Mazurek, M. Seidel, M. Kunert, K. Santos, H. von Moeller, B. Loll, J. B. Weston, A. Mainz, J. G. Heddle, R. D. Süssmuth and D. Ghilarov, *Nat. Catal.*, 2023, **6**, 52–67.
110 D. Kerwat, S. Grätz, J. Kretz, M. Seidel, M. Kunert, J. B. Weston and R. D. Süssmuth, *ChemMedChem*, 2016, **11**, 1899–1903.

111 World Intellectual Property Organization, WO2014125075A1, 2014.
112 K. Nepali, H.-Y. Lee and J.-P. Liou, *J. Med. Chem.*, 2019, **62**, 2851–2893.
113 World Intellectual Property Organization, WO2019185806A1, 2019.
114 World Intellectual Property Organization, WO2019015794A1, 2019.
115 S. Grätz, D. Kerwat, J. Kretz, L. von Eckardstein, S. Semsary, M. Seidel, M. Kunert, J. B. Weston and R. D. Süssmuth, *ChemMedChem*, 2016, **11**, 1499–1502.
116 World Intellectual Property Organization, WO2023232519A1, 2023.
117 World Intellectual Property Organization, WO2025003147A1, 2025.
118 G. Testolin, J. Richter, A. Ritter, H. Prochnow, J. Köhnke and M. Brönstrup, *Chem.–Eur. J.*, 2022, **28**, e202201297.